End-Point Free Energy Prediction using PB and MSSAS

by

Yuchen Sun

Bachelor of Science, Sun Yat-sen University, 2020

Submitted to the Graduate Faculty of the

School of Pharmacy in partial fulfillment

of the requirements for the degree of

Master of Science

University of Pittsburgh

2022

UNIVERSITY OF PITTSBURGH

SCHOOL OF PHARMACY

This thesis or dissertation was presented

by

Yuchen Sun

It was defended on

March 25, 2022

and approved by

Xiangqun Xie, Professor, School of Pharmacy

Levent Kirisci, Professor, School of Pharmacy

Junmei Wang, Associate Professor, School of Pharmacy

Zhiwei Feng, Assistant Professor, School of Pharmacy

Thesis Advisor/Dissertation Director: Junmei Wang, Associate Professor, School of Pharmacy

End-Point Free Energy Prediction using PB and MSSAS

Yuchen Sun, B.S.

University of Pittsburgh, 2022

ABSTRACT

Solvation free energy (SFE) is a basic concept used in many areas. The accurate prediction of SFE lays the foundation for binding free energy prediction and it is also useful for the calculation of logarithm of 1-octanol-water partition coefficient (logP) which is a frequently used parameter in drug discovery. In this work, the performance of ABCG2 (AM1-BCC-GAFF2) charge model as well as other two charge models, i.e., RESP (Restrained Electrostatic Potential) and AM1-BCC (Austin Model 1-bond charge corrections) on SFE prediction of 633 small molecules in water by MM-PB/GBSA was evaluated. AM1-BCC charge model has the best performance of SFE prediction using GB1, PB_DELPHI methods with root mean square error (RMSE) of 1.88 kcal/mol, and 2.70 kcal/mol, respectively. Meanwhile, ABCG2 charge model performed better using GB2 and GB5 methods with RMSE of 2.06 kcal/mol and 2.17 kcal/mol, respectively. We further explored the influence of atom radii on the prediction accuracy and yielded a set of atom radii parameters suitable for more accurate SFE prediction using ABCG2 charge model by MM-PBSA method. Then, we tuned the nonpolar model for SFE calculation. Using our new model and parameters, for 544 training set molecules, the mean signed error (MSE) and RMSE of the SFE calculation decreased from -1.59 kcal/mol to 0 kcal/mol, and 2.38 kcal/mol to 1.05 kcal/mol, respectively. We then tested the new atom radii parameters on other charge models and found the new radii parameters also outperformed old ones in SFE prediction. Finally, the new radii parameters were adopted in the prediction of protein ligand binding free energy using MM-PBSA

method. For the four systems tested, there is improved correlation between experiment and calculation results. And smaller error for absolute binding free energy were also observed, except for JNK1. We then applied the new radii parameters and adopted same approach to generate nonpolar SFE model for octanol SFE prediction. Based on that, a mix logP prediction model using physical method supported with empirical corrections was built. The superiority of our logP model was validated by smaller prediction error to drug-like molecules in ZINC database compared to other commonly used methods.

Table of Contents

List of Tables

List of Figures

List of Equations

Preface

I would like to express my deep and sincere gratitude to my mentor Dr. Junmei Wang for providing me the invaluable guidance in my research. His dedication and keen effort in helping the development of students is the sole reason that I can successfully finished my Master's study and got closer to my dream. It was my privilege and honor to work and study under the guidance of such an exceptional researcher. I would also like to thank all the other lab members in Dr. Wang's lab especially Dr. Xibing He. He taught me a lot in molecular modeling with great patience and laid the foundation of my achievements in the new field. Without his generous help, I would not make such progress as a beginner.

Finally, I would like to give special thanks to my parents and all my family members. Thank you for the selfless love and care which shape the optimistic and resilience part of my nature. I am truly grateful to your offering and sacrifice for educating me and preparing me for my future. You are the ones that I can come to when I feel low, and it is you who offer me timely help and support along the way. I would also like to extend my warmest thanks to my friends for the happiness and inspiration they bring me.

1.0 INTRODUCTION

1.1 Solvation Free Energy

Free energy is the driving force in many biological processes such as protein folding and receptor ligand binding. Solvation free energy (SFE) is the change of free energy in the solvation process. It is a crucial property which is useful in many aspects. In the drug development campaign, the accurate prediction of SFE not only enables better prediction of the binding of protein and ligand (since the binding process usually happens in the aqueous environment) but also helps the prediction of the solubility of drug candidates and guides the selection of candidates in early drug-discovery stage[1].

1.2 Free Energy Calculation Methods

The pursuit of accurate and efficient SFE calculation methods never stops. Currently, various approaches to predict the SFE are available, ranging from simple structure-based prediction models to complex alchemical perturbation methods. The Quantitative Structure Activity Relationships (QSAR) and Quantitative Structure Property Relationships (QSPR) methods are widely used methods in this field. They can achieve good prediction with relatively low computational cost. But these methods are prone to have better performance for molecules which are similar to the molecules in the training set[1]. Alchemical simulation methods like free energy perturbation (FEP) and thermodynamic integration (TI) are also used in SFE estimation, but these

methods are generally much more computationally demanding and the sampling and assessment of convergence remain a problem for users[2]. Molecular mechanics Poisson-Boltzmann surface area (MM-PBSA) calculation and molecular mechanics generalized Born surface area (MM-GBSA) calculation are among the popular and widely used methods for calculation of the SFE. The methods gain their popularity because of perfect balance between accuracy and computation cost. Compared to rigorous alchemical free energy methods like FEP or TI, MM-PBSA and MM-GBSA methods can greatly reduce the computation cost as they are based on samplings from the "end points" (the receptor-ligand complex and the free receptor and ligand) without the intermediate states[3, 4].

1.2.1 MM-PB/GBSA

In theory, the free energy of solvation process is divided into the polarization free energies and cavity, dispersion and solvent structure free energies[5]. MM-PBSA and MM-GBSA methods decompose binding free energy into several different terms: the gas phase molecular mechanics energy (ΔE_{MM}), SFE (ΔG_{solv}), and the entropy change due to the change in conformation of the molecules ($-T\Delta S$)[4]:

$$\Delta G_{bind} = \Delta E_{MM} + \Delta G_{solv} - T\Delta S$$

Equation 1 Binding free energy calculation

The SFE part can be further divided into the polar and nonpolar terms. The polar part of the SFE ($\Delta G_{PB/GB}$) is usually calculated using the Poisson-Boltzmann (PB) or Generalized Born (GB) model, while the nonpolar part (ΔG_{SA}) is estimated through solvent accessible surface area (SASA)[6].

$$\Delta G_{solv} = \Delta G_{PB/GB} + \Delta G_{SASA}$$

Equation 2 Solvation free energy calculation

In a PBSA model, the polar term is calculated by solving the PB equation, either numerically or analytically, while in a GBSA model, an alternative GB approximation of the PB model, which requires less computation time, is applied to calculate the polar term. The nonpolar term of a PBSA or a GBSA model is usually estimated by SASA to account for the cavity, dispersion and solvent structure free energies in the solvation process[7]. In most applications, the contribution due to the different conformations in gas and solvent is typically ignored. In the current drug discovery efforts, MM-PBSA and MM-GBSA methods are prominent methods in the computer-aided drug design (CADD) area with various applications including study of ligand binding[8], macromolecule interactions[9] and virtual screening[10]. Prediction of receptor-ligand binding is one of the most important topics in CADD. MM-PBSA and MM-GBSA have been extensively applied in this area as it is generally more reliable than the docking method and more practical than the extremely time-consuming alchemical methods. Further, the ability of analyzing the contribution of each individual receptor residue to the total binding free energy enables this method for more in-depth analysis of the detail about ligand-receptor interaction. Macromolecule interactions, such as protein-protein, protein-RNA/DNA interactions, are important for drug discovery as they are involved in a lot of disease mechanisms. MM-PB/GBSA is widely used and might be the best approach available for this kind of study[9].

The accuracy of SFE prediction by MM-PB/GBSA is determined by various factors[6, 11], including force fields, charge methods, the strategies of sampling, the definition of dielectric boundary in the continuum solvent model, the dielectric constant of solutes, the atom radii parameters, etc[12, 13]. In this study the following influencing factors are addressed. First of all, the different calculation methods for polar contributions can yield different results. As mentioned above, the polar part of SFE can be calculated using a PB approach or an alternative GB approach

which is more efficient in terms of computational cost. Different GB methods are also available. For example, in the AMBER program package, when it comes to the calculation of SFE, practitioners can choose GB1 (the most extensively tested version of GB model), GB2 and GB5 (newer model using the "OBC" models which improve the performance dramatically)[14]. Secondly, different approaches exist for the nonpolar part. Although the nonpolar contribution is often calculated using SASA, molecular volume is also applied to more accurately estimate the cavity term[15]. Moreover, there are several formulas developed for predicting the nonpolar part using SASA. Thirdly, the different charge methods and different radius parameters for the atoms also play critical role in the SFE calculation[16]. Restrained electrostatic potential (RESP) charge model can fit the atomic charges to the electrostatic potential calculated by quantum mechanics (QM) at the HF/6-31G* level of theory[17, 18] and it is compatible with the force fields in the AMBER family including the General AMBER Force Field (GAFF) for arbitrary organic small molecules[19]. However, in order to avoid the high computational cost of QM calculations, the semi-empirical Austin Model 1 with bond charge corrections (AM1-BCC)[20, 21] is more widely used in the simulations using GAFF because it is more efficient and less dependent on the input molecule conformation[22]. The newly introduced ABCG2 charge model was recently developed to much better reproduce SFEs through TI by adjusting BCC parameters compatible to GAFF2[22].

1.2.2 TI

TI stands for thermodynamic integration. It is one of the most popular methods used to compare the free energy difference between two states, 0 and 1. Due to the fact that it is not feasible to calculate the free energy difference just based on the simulation of the two end states[23], it is necessary to define the thermodynamic path between the end states and integrate the enthalpy

changes along the path. The simulation of the intermediate states are characterized by coupling parameter λ, which range from 0 to 1. The initial state correspond to λ = 0, while in the final state 1, λ = 1.

In this work, for the integral of the total free energy, the numerical quadrature is used as **Equation 3** (1-3) demonstrates:

$$V(\lambda) = (1-\lambda)V_0 + \lambda V_1 \quad (1)$$

$$\Delta G = G(\lambda = 1) - G(\lambda = 0) = \int_0^1 \langle \frac{\partial V}{\partial \lambda_\lambda} \rangle \, d\lambda \approx \sum W_i \langle \partial V / \partial \lambda \rangle_i \quad (2)$$

$$\frac{\partial V}{\partial \lambda} = V_1 - V_0 \quad (3)$$

Equation 3 Free energy integration using numerical quadrature

The V(λ) in equations are the mixed potential of the initial state V0 and the final state V1.

1.3 Solvation Free Energy and logP

Partition coefficient is defined as the ratio of a molecule's solubility in two immiscible solvents. The logarithm of partition coefficient (logP) between 1-octanol and water is a critical property which closely related to the solubility, permeability, ADME and affinity of the molecule to the target[24-27], thus frequently used in describing the druggability. The importance of logP among other physical chemical properties in determine the fate of drug candidates are recognized long time ago. Back in the 1960s, the calculation of logP was first reported by Fujita et.al[28, 29] and was regarded as key factors in determination of the drug ADME properties. The well-known Lipinski's rule of five[30, 31] further strengthen the idea that simple molecule descriptors like logP can be critical in predicting the druggability.

1.4 logP Prediction Methods

1.4.1 Experimental Methods

Several methods for experiment measurement of drug logP have been developed[28, 32, 33]. The shake flask method and reversed phase high performance liquid chromatography are commonly used methods[34, 35], but the experiment determination of logP has limitation when it comes to the logP prediction of molecules which are unstable in solvent. While at the same time, the difficulty to synthesis or get the compound to determine its logP remains a problem, especially in the initial stage of drug discovery, when large number of potential structures need to be screened and their physical chemical properties need to be determined[36].

1.4.2 Computational Methods

The prediction of logP using computational methods is very important alternative to the existing experimental method. With decades of development, there are a number of computational methods which adopted different underlying theoretical principles to assist researcher in prediction of compound logP. Popular commercial software like Discovery Studio, MOE, Maestro also support the logP calculation, with either open-source models (Discovery Studio supports AlogP[37]) or their own unpublished models (MOE uses both unpublished model “Labute”[38] and hybrid SlogP[39]).

The calculation methods for logP can be classified into the following three major groups: 1. Atomic based methods 2. Fragment/Compound based methods 3. Property based methods. The atomic logP is simply calculate the additive contribution of each atom of molecule in logP, an

example of such method is AlogP[37]. To get reasonable results, this method takes atom type into consideration, for example the same atom in different functional groups has different contributions. Atomic logP is not suitable for molecules with very complex structures or electronic systems which will greatly affect logP. To overcome these short comings, enhanced atomic or hybrid logP method was proposed. This method applies corrections and considers the contributions of atoms with neighbor atoms for better prediction of large systems, XlogP[40] and SlogP[39] as examples. Fragment/Compound logP (Clogp[41], KlogP[42], etc.) requires an experiment determined logP dataset which contains lots of molecules and fragments. The prediction model is then built using QSAR or other regression methods. This method tends to have better performance for large molecules which is similar to the training set. The last method is property-based method, which including the logP prediction using 3D structure representation and topological descriptors[43]. The former one can be further divided into empirical approaches, quantum chemical semiempirical method and continuum solvation model based method, molecular dynamic (MD) simulation based method, lattice energy based method and MLP methods. Procacci et.al conducted logP estimation using a non-equilibrium alchemical technique called non equilibrium switching (NES) for the drug like molecules in the SAMPL6 challenge and was able to achieve MUE of 1.06 and R of 0.79 for training set molecules which is among the top ranked submissions[44].

Generally speaking, the complexity of calculation increases from atomic based method to property-based method, while theoretically, the accuracy also increases. Although simple methods like AlogP[37] and ClogP[41] are popular and widely used, these methods are not very accurate especially for large and flexible molecules. The past decades have seen a trend of increase in molecular weight of approved drug molecules[45]. According to the review by Shultz[46], in general, ClogP will overestimate logP for molecules which were approved by FDA after the

publication of the famous “Lipinski rule of five”. A hypothesis to this phenomena is that the logP calculation error is due to the high flexibility of such molecules which will bury polar atoms and result in collapse of hydrophobic groups that fragment methods will not address[47]. For logP prediction using properties based “physical” methods, the accurate prediction is generally based on theoretically rigorous interpretation of solvation process. For example, high level quantum chemical (QM) calculations with implicit solvent parameterization can achieve relatively good accuracy and those methods are the best ranking physical methods in the SAMPL6 challenge[48]. Nevertheless, such methods require a descent amount of computational time, making the it less attractive.

1.5 Aim

1.5.1 Test the ABCG2 Charge Model with MM-PB/GBSA Methods

As aforementioned, different calculation methods for polar part of SFE, various nonpolar SFE models as well as different charge models applied will pose significant influence to the SFE prediction results. The first aim is to evaluate the newly proposed ABCG2 charge model and explore the relationship between charge model, calculation method and prediction accuracy. In this work we compare the application of the new ABCG2 charge as well as other widely used charge models (AM1-BCC, RESP) combined with GAFF2 on the prediction of the SFE of the small molecules by MM-PB/GBSA. The prediction accuracy using different polar SFE calculation methods was also explored simultaneously. For each charge model, three different

implementations of GB method and two implementations of PB method were adopted when conducting the SFE prediction.

1.5.2 Improve the Binding Free Energy Prediction using ABCG2 Charge Model Combined with MM-PBSA

Binding of ligand and receptor is the key reason for most drug to have their effect. The protein ligand binding free energy is important for the affinity ranking of the compounds for a given target, which can guide drug discovery. Thus, the accuracy prediction of binding free energy is the central topic for computer aided drug design.

SFE is essentially related to binding free energy. Consequently, we hope to improve the overall performance of binding free energy prediction by minimizing the errors introduced in SFE calculation. As ABCG2's parameters were specially optimized based on TI calculation of small molecule SFE[22], in this work, we conducted optimization for PB atom radii to achieve better results of SFE calculation using MM-PBSA and the ABCG2 charge model. Moreover, the new PB atom radii were also evaluated against the AM1-BCC and RESP charge methods. We hope the new PB atom radii can universally improve the performance of SFE prediction using the PBSA methods regardless of charge method being used.

There are eight drug targets that have been extensively used as a golden standard to test the performance of new free energy calculation methods[49-51]. According to the study by Hao et al[51] which evaluated the accuracy of MM-PBSA calculation in predicting the protein ligand binding free energy of the eight drug targets, there are four systems, namely, β-Secretase 1(BACE1)[52], C-Jun N-terminal kinase 1 (JNK1)[53], P38[54], protein tyrosine phosphatase 1B (PTP1B)[55] have relatively large deviation and poor correlation between experiment results and

calculation results. Consequently, we wanted to test our new radii parameters and nonpolar SFE models on these four difficult systems to see if the protein ligand binding free energy calculation will be improved.

1.5.3 Build a Mixed logP Prediction Model

In this study, we proposed a mixed logP prediction method which established by physical modeling supported with empirical correction. From thermodynamic point of view, logP is proportional to the Gibbs free energy of transfer a molecule from water to octanol as the **Equation 4** shows:

$$-RTln10 * logP = \Delta G_{transfer}[56]$$

Equation 4 Relationship between logP and Gibbs free energy of transfer

The R in the equation represent the gas constant ($8.314 J \cdot mol^{-1} \cdot K^{-1}$), while T is the thermodynamic temperature (K). Consequently, logP can be calculated by the solvation free energy (SFE) of molecule in water and octanol:

$$logP = \frac{\Delta G_{water\ SFE} - \Delta G_{octanol\ SFE}}{RTln10}$$

Equation 5 logP calculation using solvation free energy

Our method first used PB solver DelPhi[57, 58] to calculate the polar part of SFE. The nonpolar SFE model was then generated by fitting the difference of experimental SFE and polar part of SFE with solvent accessible surface area (SASA). Because our newly introduced logP calculation method is from a physical point of view, we hope our method is superior to QSPR methods in logP prediction and less computational demanding than rigorous alchemical methods the same time.

2.0 METHODS

2.1 Data Preparation

The experimental data of the SFE of molecules in water and 1-octanol were obtained from the FreeSolv v0.52 database[59] and Minnesota Solvation Database version 2012[60]. The structures of solute molecules were taken from the database in mol2 format and imported to Schrodinger Maestro to check the structures manually. In total, 633 small molecules with their structures and experimental SFE in water were compiled, while 247 molecules' structures and experimental SFE in 1-octanol were obtained.

After obtaining all the data, the geometry optimization for all the small molecules was conducted using Gaussian 16[61] with Hartree-Fock method and 6-31G* basis set. The Gaussian output files were used to generate residue topology and additional force field parameter files by Antechamber[53] using the GAFF2 force field. For RESP charge model, the RESP program in Amber Tools was applied to derive charges by fitting electrostatic potential generated at the HF/6-31G* level. For AM1-BCC and ABCG2 charge models, the SQM (semiempirical quantum mechanics) module in Amber Tools was performed to generate AM1 Mulliken charge, and then bond charge correction was applied using the corresponding BCC terms, respectively.

For each small molecule, a cubic box with a single solute molecule solvated in explicit TIP3P water[62] was created using the TLEAP module in Amber Tools. The minimum distance between any part of the solute and the edge of the box was set to 12 Å to avoid image violations. The parameters and coordinates were saved for the next step simulation.

2.2 Minimization and Molecular Dynamics Simulation.

The minimization and molecular dynamics (MD) simulation were conducted using the Pmemd.mpi module in AMBER18[14]. Both the steepest descent and conjugate gradient methods were used to perform the minimization. The number of cycles of steepest descent was set to 1000, and then switched to conjugate gradient method and ran another 1000 cycles.

The MD simulation was separated into heating, equilibration and production phases. First, the system was heated from 0 K to 298.15 K within 100,000 steps with a time step of 0.001 ps. Then 0.1 ns equilibration and 5.0 ns production phases of MD were carried out with the temperature kept at 298.15 K using Langevin dynamics[63] with collision frequency equaled to 2.0 ps^{-1}. For the whole MD simulation, periodic boundary condition was applied, the pressure was set to 1.0 bar with 1.0 ps pressure relaxation time. The SHAKE constraints for bonds involving hydrogen were applied to the system. The trajectories were saved every 10 ps for later MM-PB/GBSA calculations.

2.3 MM-PBSA and MM-GBSA Calculation for HFE

The trajectory files of MD simulation in the production period were used to generate snapshots of each solute (with water stripped) using the Cpptraj module in Amber Tools[64]. All MM-PB/GBSA calculations were performed using an internal program, mmpbsa, which calls Sander and Pmemd programs in the AMBER package as well as Delpha 95 software[57, 58] to calculate different energy terms (ΔE_{MM} and $\Delta G_{PB/GB}$). The HFE (hydration free energy) of the 633 molecules was calculated using the topology and coordinate files generated from GAFF2 force

field parameters and three different charge methods namely RESP charge, AM1-BCC charge and ABCG2 charge. And for each of the three charge methods, different ways to calculate polar contribution terms were applied: GB1, GB2, GB5, PB_DELPHI[57, 58] (PB calculation using DelPhi). The nonpolar contribution was estimated using SASA calculated by an internal program, the probe radius adopted here is the typical value 1.4Å. The accuracy of the final HFE prediction was demonstrated using a set of statistical metrics: root-mean-square-error (RMSE), mean unsigned error (MUE), mean signed error (MSE), prediction index (PI) and Pearson's correlation coefficient R.

2.4 Thermodynamic Integration Calculation

Thermodynamic integration (TI) is a widely used path-based approach for alchemical free energy calculations[23, 50, 65-68]. The principle of TI method has been well described in many references[69-71]. We calculated the absolute hydration free energy using TI methods for 642 compounds that have measured values. Those molecules were described by GAFF2 force field with ABCG2 charge model.

TI simulations in both the aqueous solution and gas phase environments were conducted for each compound using 9 λ-windows which mixed the potentials of the two states (labeled as "1" and "0") with the following coefficients: 0.01592, 0.08198, 0.19331, 0.33787, 0.5, 0.66213, 0.80669, 0.91802, 0.98408, mimicking a Gaussian quadrature. The weights of the contribution to ΔG are 0.04046, 0.09032, 0.13031, 0.15617, 0.16512, 0.15617, 0.13031, 0.0932, and 0.04046, for the 9 λ-windows, respectively. The hydration free energy of a compound, ΔG_{hyd} was computed in

two TI processes, the de-charging ($\Delta G_{hyd}^{decharge}$) and atom disappearing $\Delta G_{hyd}^{disappear}$, and $\Delta G_{hyd} = \Delta G_{hyd}^{decharge} + \Delta G_{hyd}^{disappear}$. For the de-charging procedure, "1" state is the molecule described with full set of force field parameters, and "0" state is the "1" with all charges being set to 0. For the subsequent disappearing TI step, "1" is the same as "0" in the de-charging step, while "0" is the same as "1" of this TI step but with the potential well depths of all solute atoms being set to 0. $\Delta G_{hyd}^{decharge}$ and $\Delta G_{hyd}^{disappear}$ represent the polar and nonpolar contributions of the solvation process.

The MD simulation system consists of 1 copy of solute which is described by GAFF2[19], and a certain number of TIP3P water molecules in a rectangle box with any atom of the solute being apart from the edges of the box at least 12 Å. Prior to the TI processes, the system was equilibrated with a 600-picosecond NTP (constant particle, temperature and pressure) simulation with periodic boundary condition being applied. For each MD simulation in TI calculations, the temperature was kept at 298 K using Langevin dynamics with the collision frequency gamma_ln being set to 2.0. The time step of 1femptosecond was applied to integrate the equation of motion. For each λ-window, 1250-picosecond NTP simulation was performed and 250 snapshots were collected. ΔG (DV/DL) was calculated by averaging the DV/DL values of the last 150 snapshots. For post-MD analysis, we applied an internal program to conduct statistical analysis of DV/DL and calculate $\Delta G_{hyd}^{decharge}$, $\Delta G_{hyd}^{disappear}$, and ΔG_{hyd}.

2.5 The Procedure of ABCG2 Evaluation and PB Radii Optimization

After the charge method and calculation method evaluation and the TI calculation, the PB radii parameters were tuned for better performance of HFE prediction using MM-PBSA method with ABCG2 charge. The PB radii parameters are used in PB calculations using DelPhi[57, 58], and the result of the calculation is used to estimate the polar part of the SFE. Because TI calculation with ABCG2 charge model already demonstrated good accuracy in the prediction of SFE of small molecules in various solvents[22], while there are few experiment data for polar part of SFE available, and TI calculation can separate the SFE into polar part and nonpolar part. So, the optimization of PB radii parameters is to reproduce the TI HFE calculation results. Based on the HFE calculation using TI, all the molecules with difference between calculation results and experiment results larger than 1.5 kcal/mol were excluded from the training dataset. In total 89 molecules were excluded and 544 molecules retained. After that, the molecules were divided into different classes based on their primary function groups, and MSE, MUE, RMSE of experiment value versus calculation value were obtained for each function group individually. The molecules with multiple functional groups were excluded. The groups with large systematic error (MSE, MUE or RMSE larger than 1.40 kcal/mol) were adjusted and new reasonable PB radii parameters which yield smaller error of polar HFE prediction were adopted. A new atom type for the oxygen in nitro functional groups was also defined in the procedure as we found that if it shares the same radius with other carbonyl oxygens, the error of HFE is very large. Meanwhile, for molecules that bear charge, the new atom type ***oi***, ***hn1***, ***hn2***, ***hn3*** were also defined. The general procedure for PB radii optimization is described as follows. First, we found out the principal atom type behind each functional group; we then conducted systematic search to optimize the PB radii for the selected atom type. Next, we calculated the new PB_DELPHI of the series of molecules with the

selected atom type and got the MSE, MUE and RMSE between PB_DELPHI and TI_polar. We conducted PB radii optimization and PB calculation iteratively until the MSE, MUE and RMSE fall below the acceptable standard (approximately 1.40 kcal/mol). We followed the order of atom types ***o***, ***on***, ***oh***, ***os***, ***cl***, ***ss***/***sh***,***c1***, ***f***, ***p5***, ***s6*** to adjust the parameters step by step and the optimized parameters would be applied in the subsequential optimizations (Figure S1 and Table S1). The atom types for different functional groups are listed in Table S1. The general consideration for parameter adjustment is that we first try to adjust the functional groups which occur in multiple functional groups (i.e., carbonyl group not only occur in ketones but also occur in aldehydes, esters, amides), then those functional groups with multiple atom types were tuned (Figure S1).

In order to make our new set of PB radii parameters more unified and concise, those atom types with similar environment and can reach reasonable results were assigned the same radii values when possible. For example, thiols and thiol ethers have different atom types (***ss*** and ***sh*** respectively), but their radii parameters were tuned simultaneously and kept the same. For nitro functional group, two kinds of atom types were involved, namely ***on*** (newly defined for oxygen) and ***no*** (for nitrogen). Oxygen radii plays critical role in the calculation because compared to nitrogen, oxygen atoms are more exposed to solvent. Thus, its radius has bigger impact on SFE calculation results. As a result, the change in ***on*** (an oxygen atom type) lead to a more dramatic change in the calculation. So, the ***no*** (the nitrogen atom type in nitro) parameter remained unchanged to keep our parameter set unified. Although further optimization can be done for ***no*** atom type and better results can be achieved, this was not done because achieving both accurate and concise is our priority.

After the optimization for PB radii was finished, PB_DELPHI was calculated for all the 544 molecules. The nonpolar part of HFE for the molecules was calculated by experimental HFE

subtract calculated PB_DELPHI. As mentioned above, the nonpolar part of SFE is related to cavity, dispersion and solvent structure free energies[7]. Traditionally the sum of the three terms is usually estimated by solvent accessible surface area (SASA). The new nonpolar HFE model was generated by fitting the nonpolar HFE with WSAS (weighted solvent accessible surface area) which correspond to the cavity formation of the solvation process and the Van der Walls interaction (dispersion term) in the solvation process.

Finally, after all the parameter optimization is done and the new nonpolar model was established, the HFE of both the training set molecules (394 molecules, excluding the molecules with multiple functional groups) and all the 544 molecules were calculated again.

2.6 Validation of New Radii Parameters on the Binding Free Energy Prediction

Wang et al. applied Schrodinger's FEP+ program to calculate relative binding free energies for a set of 8 protein systems[49]. Recently, we evaluated the "Gold Standard" benchmark set using both GPU-TI implemented in AMBER18 and MM-PBSA-WSAS methods[50, 51]. Although the MM-PBSA-WSAS method outperformed the Glide docking approach, for some systems including BACE1, JNK1, P38 and PTP1B, the performance measured by correlation coefficient R and RMSE of absolute binding free energies is not satisfactory. As we have significantly improved the accuracy of solvation free energy calculations, it is expected that the new PBSA model can also boost the performance of protein-ligand binding free energy calculations. We evaluated the new PBSA model for the four aforementioned protein systems.

The MD protocol of sampling protein-ligand conformations for MM-PBSA-WSAS free energy calculations was detailed in our previous publication[51]. In this work, for each system we

evenly selected 100 snapshots from the sampling phase to the perform MM-PBSA-WSAS analysis using both the old and new PBSA models. Specifically, an internal program was applied to calculate the MM-PBSA-WSAS free energies of the complex and the binding free energy between a ligand and its receptor. The polar part of the solvation free energy was calculated using Delphi 95 software[57, 58], and the nonpolar part was estimated by scaling the solvent accessible surface area as described elsewhere[4, 72]. The conformational entropy term was predicted using WSAS, a weighted solvent-accessible surface area method[73]. The exterior dielectric constant of PBSA calculations was set to 80.0, the dielectric constant of water, while the interior constant was set to 1 for all systems except for PTP1B for which a dielectric constant of 4 was used, which can better describe the dielectric constant of the charged ligands.

2.7 Nonpolar Model for Octanol SFE and logP Calculation

The previous steps revealed the importance of PB radii parameters in the free energy calculation and yielded a set of radii parameters compatible with the newly developed ABCG2 charge model[22]. In logP calculation, the radii parameters as well as the nonpolar model for the SFE calculation in water were adopted from the previous results. In the calculation of SFE in octanol, I continue to use the aforementioned set of radii parameters optimized using water SFE and by changing the nonpolar SFE model, we got good consistency between experiment determined SFE and calculated SFE in octanol. The nonpolar model was generated by conducting the regression between experiment minus polar SFE (PB) and the surface area (MSSAS).

Finally, the nonpolar model of water and octanol SFE and the PB radii parameters were tested on the prediction of logP of 156 molecules which present in both water and octanol SFE dataset.

Apart from that, our logP calculation method was further validated through the logP prediction of drug like molecules from ZINC dataset.

3.0 RESULTS

3.1 The Performance of Three Charge Models on SFE Calculation with the Default Radius Parameters

The results of SFE calculation using different combinations of charge models and calculation methods were explored. There are three charge models applied and four different PB/GB calculation methods, so in total 12 combinations were utilized. For each combination, a set of statistical metrics (including MSE, MUE and RMSE) used to evaluate the accuracy were obtained. As **Table 1** shows, the ABCG2 charge model outperformed its counterparts RESP and AM1-BCC charge model in SFE calculation using GB2 and GB5 model with RMSE of 2.06 kcal/mol and 2.17 kcal/mol, respectively. ABCG2 charge also yielded best predictive index (PI) and Pearson's correlation coefficient (R) in calculation using PB_DELPHI[57, 58] (PI = 0.91, R = 0.90). The AM1-BCC charge model achieved better results in GB1 and PB_DELPHI calculation with RMSE of 1.88 kcal/mol and 2.70 kcal/mol, respectively.

Table 1. The comparison of three charge models on SFE prediction

The performance of RESP, AM1-BCC and ABCG2 charge model with different polar SFE calculation methods on SFE prediction. The unit of MSE, MUE and RMSE is kcal/mol.

	RESP charge					AM1-BCC charge					ABCG2 charge				
Calculation method	MSE	MUE	RMSE	PI	R	MSE	MUE	RMSE	PI	R	MSE	MUE	RMSE	PI	R
GB1	-0.21	1.58	2.15	0.84	0.84	0.20	1.32	1.88	0.88	0.88	-0.78	1.54	2.10	0.87	0.88
GB2	0.42	1.66	2.28	0.83	0.82	0.98	1.68	2.28	0.85	0.85	-0.02	1.49	2.06	0.84	0.86
GB5	0.59	1.77	2.39	0.80	0.80	1.14	1.77	2.44	0.82	0.83	0.21	1.60	2.17	0.81	0.83

PBDELPHI	-1.35	1.97	2.80	0.88	0.87	-1.00	1.76	2.70	0.90	0.88	-2.13	2.30	3.39	0.91	0.90

3.2 The Result of Polar Part of SFE after Adopting the New PB Radii Parameters

In order to quickly improve the overall performance of the MMPBSA calculation using GAFF2 force field and ABCG2 charge model, only the functional groups with large systemic error (approximately larger than 1.40 kcal/mol) between TI_polar and PBDELPHI were adjusted in this study. There are 27 functional groups adjusted, alkynes, nitriles, aliphatic ring + chloride, aromatic ring + chloride, aliphatic ring + bromide, aromatic ring + bromide, hydrocarbon + iodide, ethers, alcohols, alkene + alcohols, phenols, ketones, aldehydes, esters, nitro compounds, nitrooxy compounds, amides, thioethers, thiols, aliphatic chain + fluorine, aromatic ring + fluorine, phosphoryl, sulfone, primary, secondary and tertiary ammoniums and carboxylates were adjusted in this study. Due to the fact that some functional groups share the same atom type, in total 12 atom types (***c1***, ***o***, ***oh***, ***os***, ***f***, ***cl***, ***br***, ***i***, ***ss***, ***sh***, ***p5***, ***s6***) were adjusted and 5 new atom type (***on***, ***hn1***, ***hn2***, ***hn3***, ***oi***) was defined. As **Table 2**, **Table 3**, **Figure 1**, and **Figure 2** shows, the mean MSE, MUE and RMSE of the functional groups improved significantly after adopting the new PB radii parameters (**Table S6**). The MSE, MUE, RMSE of total 394 training set (excluding molecules with multiple functional groups) molecules are -0.67 kcal/mol, 0.83 kcal/mol, 1.02 kcal/mol respectively. While the previous MSE, MUE, RMSE are -1.72 kcal/mol, 1.77 kcal/mol, 2.23 kcal/mol respectively. The PI and R almost kept the same with the previous results with some minor improvement.

Table 2 Comparison of TI polar and PB_DELPHI using ABCG2 and old radii

The comparison between polar part of TI calculation of HFE and PB_DELPHI using ABCG2 charge model and old atom radii. The unit of MSE, MUE and RMSE is kcal/mol.

Subclass	Number	MSE	MUE	RMSE	PI	R
Non-cyclic alkanes	25	-0.15	0.15	0.16	-0.43	-0.54
Cycloalkanes	9	-0.22	0.22	0.23	0.18	0.47
Alkenes	22	-1.04	1.04	1.09	0.94	0.97
Alkynes	6	-1.68	1.68	1.68	0.71	0.46
Aromatic hydrocarbons	36	-1.12	1.12	1.24	0.97	0.98
Aliphatic chain + chloride	22	-2.6	2.6	2.78	0.97	0.96
Aromatic ring + chloride	24	-2.94	2.94	3.02	0.97	0.97
Aliphatic chain + bromide	14	-1.09	1.09	1.25	0.67	0.86
Aromatic ring + bromide	4	-1.28	1.28	1.33	0.91	0.99
Hydrocarbon + iodide	10	-1.22	1.22	1.26	0.94	0.98
Ethers	14	-1.92	1.92	2.32	0.94	0.98
Alkyl alcohols	25	-1.89	1.89	2.38	0.96	1
Alkene + alcohols	3	-3.04	3.04	3.04	0.81	0.81
Phenols	17	-2.01	2.01	2.03	0.93	0.9
Ketones	19	-1.91	1.91	1.99	0.98	0.97
Aldehydes	10	-2.43	2.43	2.44	0.1	0.06
Esters	34	-3.23	3.23	3.5	0.86	0.99
Amines	25	0.31	0.53	0.76	0.97	0.96
Anilines	8	-1.23	1.23	1.27	0.98	0.98
Pyrazines and pyridines	22	-1.02	1.02	1.15	0.92	0.94
Nitriles	5	-1.23	1.23	1.28	0.07	0.12
Nitro compounds	6	-3.12	3.12	3.13	0.99	0.91
Nitrooxy compounds	8	-4.84	4.84	5.26	0.96	0.99
Amides	5	-2.23	2.23	2.24	0.91	0.99
Thioethers	8	-1.54	1.54	1.58	0.75	0.63
Thiols	4	-1.38	1.38	1.38	0.96	0.76
Aliphatic chain + fluorine	3	-1.48	1.48	1.51	1	0.97
Aromatic chain + fluorine	2	-2.22	2.22	2.23	1	1
Phosphoryl	2	-5.04	5.04	5.16	-1	-1
Sulfone	2	-6.7	6.7	6.88	-1	-1
Sum	394	-1.72	1.77	2.23	0.93	0.93

Table 3 Comparison of TI polar and PB_DELPHI using ABCG2 and new radii

The comparison between polar part of TI calculation of HFE and PB_DELPHI using ABCG2 charge model and new atom radii. The unit of MSE, MUE and RMSE is kcal/mol.

Subclass	Number	MSE	MUE	RMSE	PI	R
Non-cyclic alkanes	25	-0.15	0.15	0.16	-0.42	-0.53

Cycloalkanes	9	-0.22	0.22	0.23	0.18	0.47
Alkenes	22	-1.04	1.04	1.09	0.94	0.97
Alkynes	6	-1.29	1.29	1.29	0.58	0.31
Aromatic hydrocarbons	36	-1.12	1.12	1.23	0.97	0.98
Aliphatic chain + chloride	22	-0.94	0.94	1.1	0.95	0.97
Aromatic ring + chloride	24	-1.53	1.53	1.56	1	0.99
Aliphatic chain + bromide	14	-0.8	0.8	0.98	0.62	0.86
Aromatic ring + bromide	4	-1.17	1.17	1.19	0.91	0.99
Hydrocarbon + iodide	10	-0.88	0.88	0.94	0.85	0.97
Ethers	14	-0.6	0.77	1.08	0.95	0.98
Alkyl alcohols	25	0.35	0.6	0.75	0.96	0.99
Alkene + alcohols	3	-0.95	0.95	0.97	0.81	0.4
Phenols	17	-0.75	0.75	0.81	0.91	0.86
Ketones	19	-0.09	0.34	0.53	0.98	0.97
Aldehydes	10	-0.56	0.56	0.58	0.35	0.43
Esters	34	-0.89	0.89	1.08	0.86	0.98
Amines	25	0.3	0.53	0.74	0.95	0.96
Anilines	8	-1.26	1.26	1.3	0.98	0.97
Pyrazines and pyridines	22	-1.01	1.01	1.13	0.92	0.95
Nitriles	5	-1.15	1.15	1.22	0.07	0.04
Nitro compounds	6	-0.16	0.22	0.3	0.8	0.85
Nitrooxy compounds	8	-1.52	1.52	1.86	0.98	0.99
Amides	5	0.65	0.65	0.75	0.9	0.98
Thioethers	8	-0.66	0.7	0.81	0.8	0.66
Thiols	4	-0.51	0.51	0.52	0.47	0.67
Aliphatic chain + fluorine	3	-0.28	0.28	0.33	1	1
Aromatic chain + fluorine	2	-1.21	1.21	1.22	1	1
Phosphoryl	2	-0.67	0.9	1.13	-1	-1
Sulfone	2	-0.65	1.05	1.23	-1	-1
Sum	394	-0.67	0.83	1.02	0.96	0.96

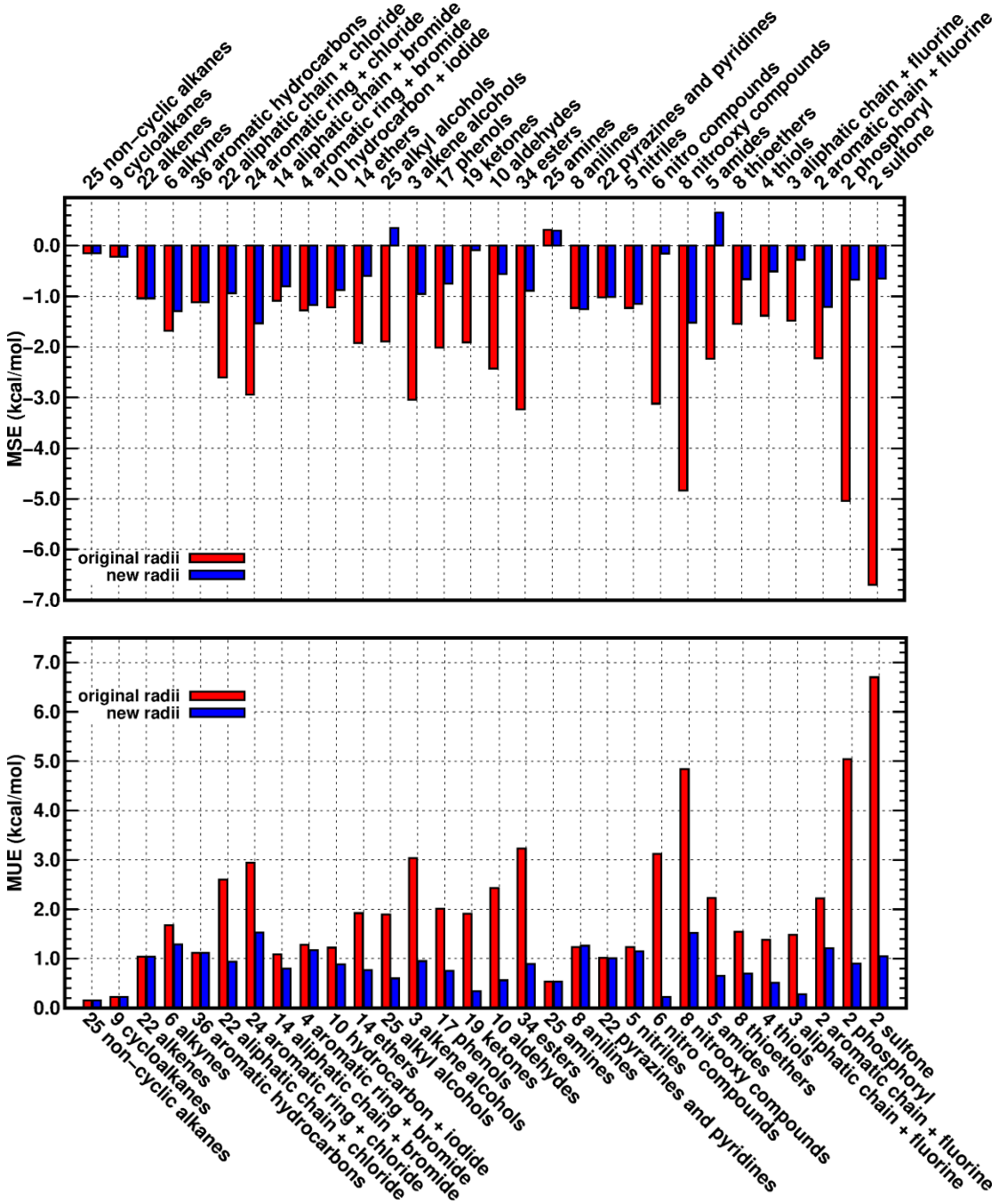
25 non-cyclic alkanes
9 cycloalkanes
22 alkenes
6 alkynes
36 aromatic hydrocarbons
22 aliphatic chain + chloride
24 aromatic ring + chloride
14 aliphatic chain + bromide
4 aromatic ring + bromide
10 hydrocarbon + iodide
14 ethers
25 alkyl alcohols
3 alkene alcohols
17 phenols
19 ketones
10 aldehydes
34 esters
25 amines
8 anilines
22 pyrazines and pyridines
5 nitriles
6 nitro compounds
8 nitrooxy compounds
5 amides
8 thioethers
4 thiols
3 aliphatic chain + fluorine
2 aromatic chain + fluorine
2 phosphoryl
2 sulfone
MSE (kcal/mol)
0.0
−1.0
−2.0
−3.0
−4.0
−5.0
−6.0
−7.0
original radii
new radii
MUE (kcal/mol)
7.0
6.0
5.0
4.0
3.0
2.0
1.0
0.0
original radii
new radii
25 non-cyclic alkanes
9 cycloalkanes
22 alkenes
6 alkynes
36 aromatic hydrocarbons
22 aliphatic chain + chloride
24 aromatic ring + chloride
14 aliphatic chain + bromide
4 aromatic ring + bromide
10 hydrocarbon + iodide
14 ethers
25 alkyl alcohols
3 alkene alcohols
17 phenols
19 ketones
10 aldehydes
34 esters
25 amines
8 anilines
22 pyrazines and pyridines
5 nitriles
6 nitro compounds
8 nitrooxy compounds
5 amides
8 thioethers
4 thiols
3 aliphatic chain + fluorine
2 aromatic chain + fluorine
2 phosphoryl
2 sulfone

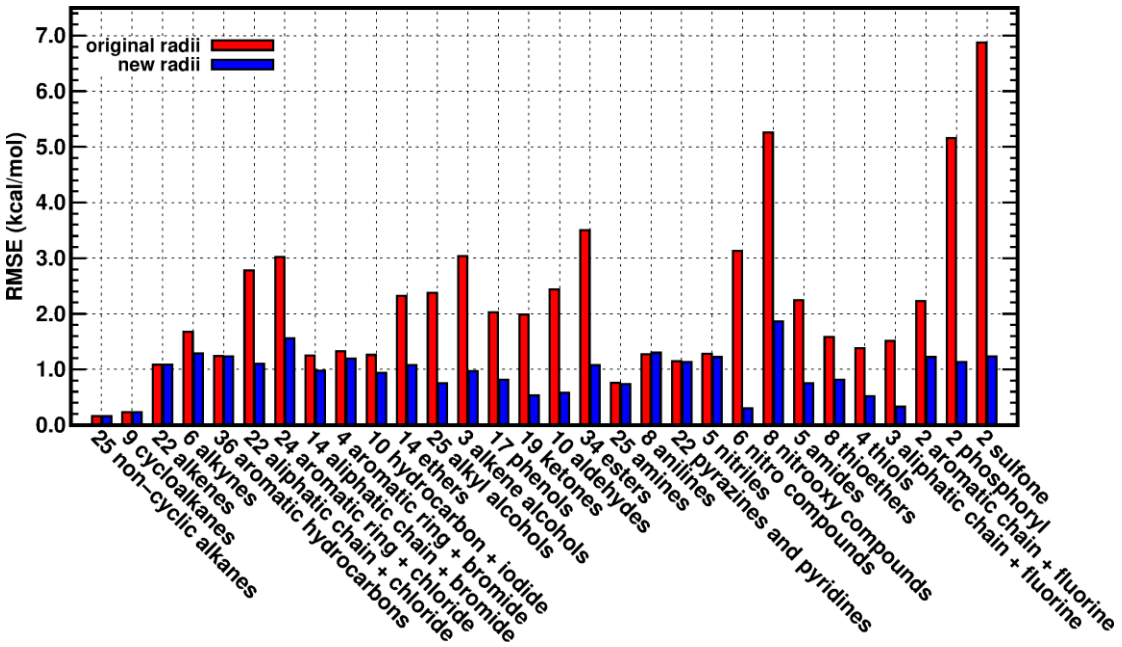

Figure 1 Comparisong of TI polar and PB_DELPHI using ABCG2 charge before and after radii optimization

The comparison of MSE, MUE and RMSE between TI polar and PB_DELPHI calculation using ABCG2 charge model before and after adjustment of atom radii. The results from original PB atom radii are in red color, and the results from updated PB atom radii are in blue color.

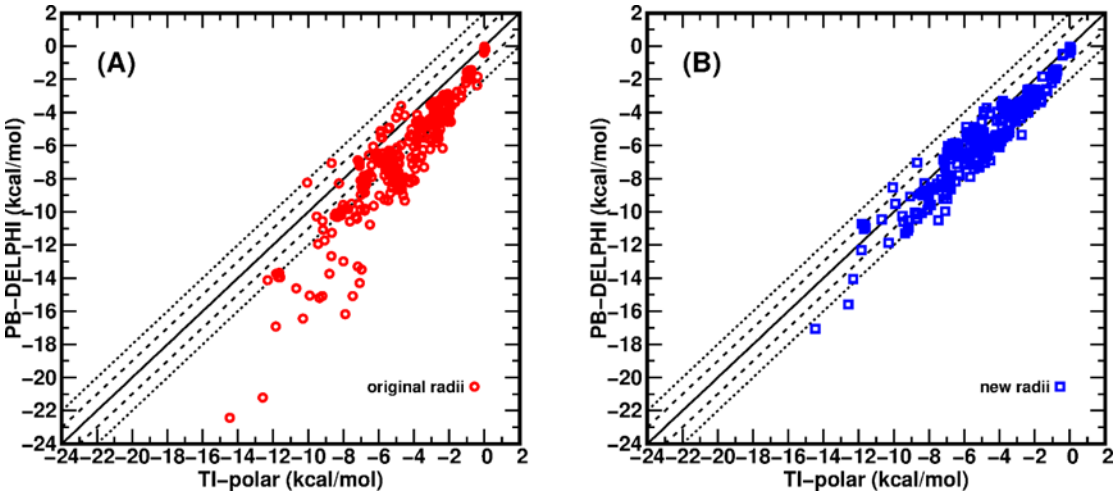

Figure 2 Comparison between TI polar and PB_DELPHI using ABCG2 with original and new radii

A, The polar part of TI calculation of HFE of small molecule vs the PBDELPHI calculation results with ABCG2 and original radii (red circles). B, The polar part of TI calculation of HFE of small molecule vs the PBDELPHI calculation results with ABCG2 and updated radii (blue squares). The lines are eye-guided lines for ideal

matching of calculation vs. experiment (solid line), with error of ±1 kcal/mol (dashed line), and with error of ±2 kcal/mol (dotted line), respectively.

3.3 New Nonpolar SFE Model

As aforementioned, the new nonpolar SFE model was generated by fitting the nonpolar HFE with MSSAS. Least square fitting and regression was conducted between nonpolar HFE (experimental HFE minus TI_polar) and MSSAS and two nonpolar models were generated accordingly. In the model validation process using the four protein ligand systems (BACE1, JNK1, P38, PTP1B), we found that both models have their advantages and disadvantages in predicting the binding free energy of protein and ligands. So, apart from the aforementioned two models, a series of models which has intermediate coefficient and constant were generated. In total nine models were tested on the prediction of protein ligand binding free energy and the model which has balanced performance were selected. The final model for nonpolar SFE we got was as **Equation 6** shows:

$$SFE_{nonpolar} = 0.0055 \times MSSAS + 1.12$$

Equation 6 Nonpolar model for SFE calculation in water

3.4 The Performance of MM-PBSA Calculation Using New Radii Parameters & Nonpolar SFE Model and ABCG2 charge

The performance of MM-PBSA calculation using new PB radii and nonpolar SFE model with ABCG2 charge model for training set molecules and all the 544 molecules were evaluated

respectively. As **Figure 3** and **Figure 4** demonstrated, for the training set (excluding molecules with multiple functional groups) which contains 394 molecules, the MSE improved from -1.19 kcal/mol to 0.07 kcal/mol, MUE improved from 1.43 kcal/mol to 0.60 kcal/mol, while RMSE decreased from 1.98 kcal/mol to 0.85 kcal/mol. The MSE, MUE, RMSE for all the 544 molecules decreased from -1.59 kcal/mol to 0 kcal/mol, 1.77 kcal/mol to 0.75 kcal/mol, 2.38 kcal/mol to 1.05 kcal/mol as **Figure 5** demonstrated.

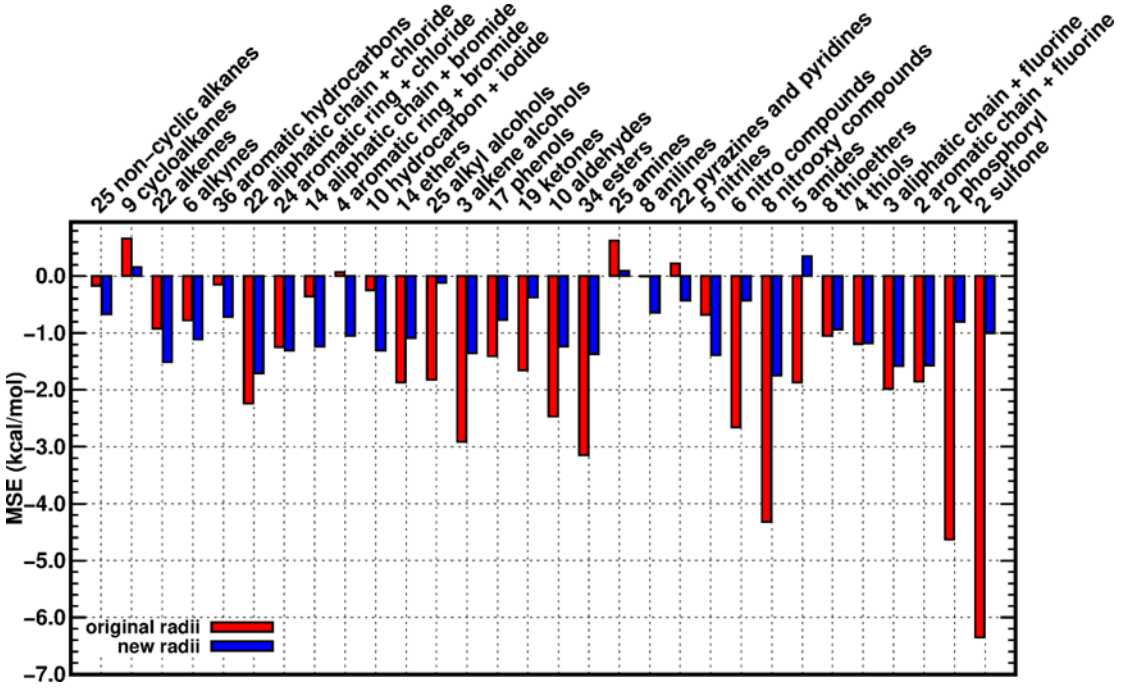

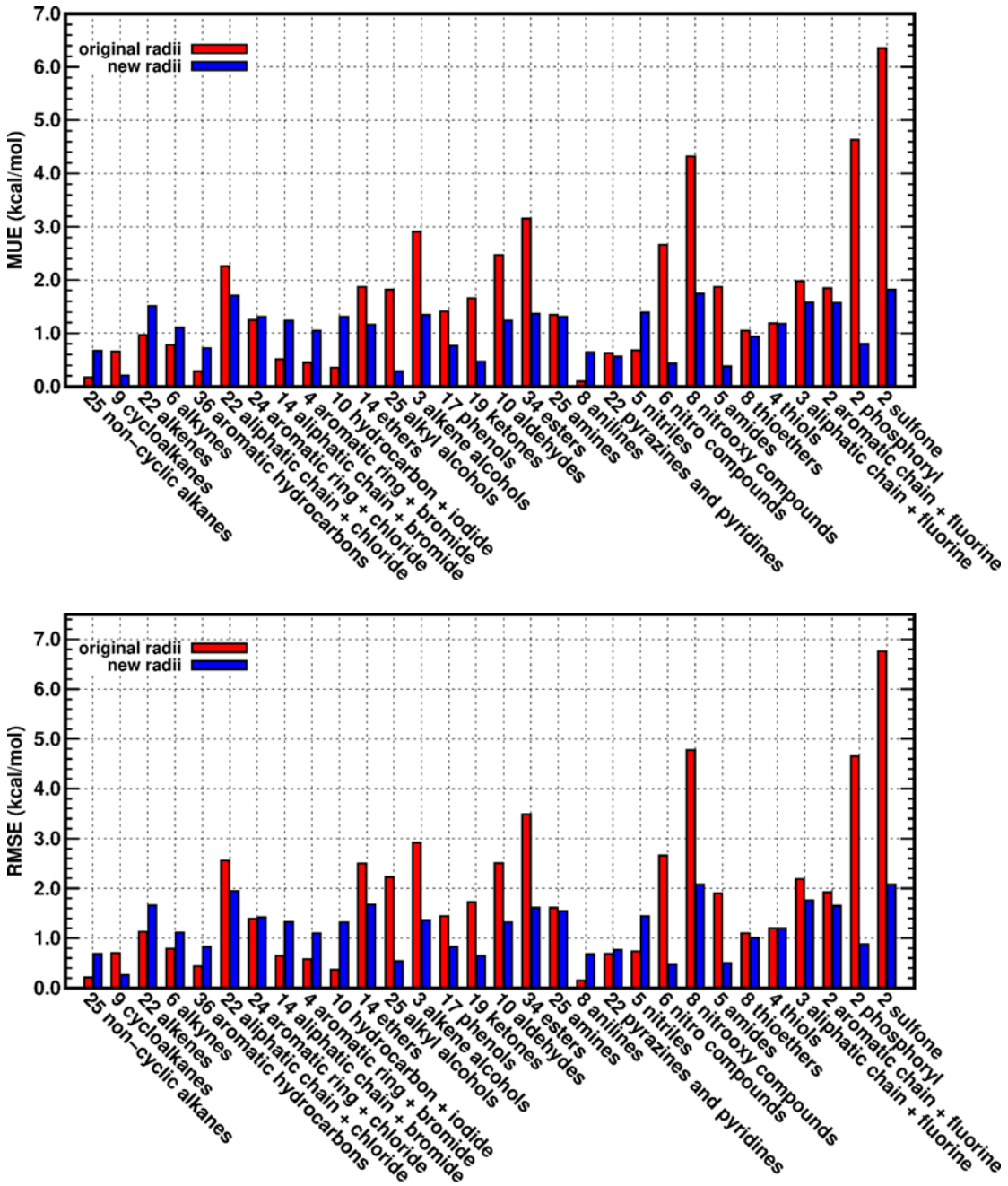

Figure 3 Comparisong of SFE calculation using ABCG2 charge before and after radii optimization

The comparison of MSE, MUE and RMSE of SFE calculation for training set molecules (excluding molecules with multiple functional groups) using ABCG2 before and after adjustment of atom radii. The results from original PB atom radii are in red color, and the results from updated PB atom radii are in blue color.

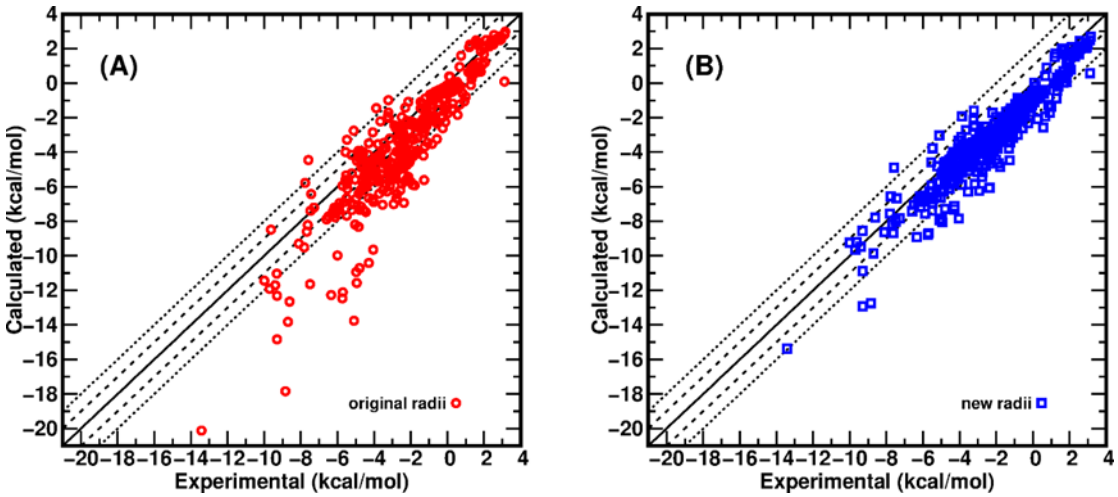

Figure 4 Comparison between experimental SFE and calculated SFE using ABCG2 with original and new radii

A, The experiment SFE of training set molecules (excluding molecules with multiple functional groups) vs the calculated SFE with ABCG2 and original radii (red circles). B, The experiment SFE of training set molecules (excluding molecules with multiple functional groups) vs the calculated SFE with ABCG2 and updated radii (blue squares). The lines are eye-guided lines for ideal matching of calculation vs. experiment (solid line), with error of ±1 kcal/mol (dashed line), and with error of ±2 kcal/mol (dotted line), respectively.

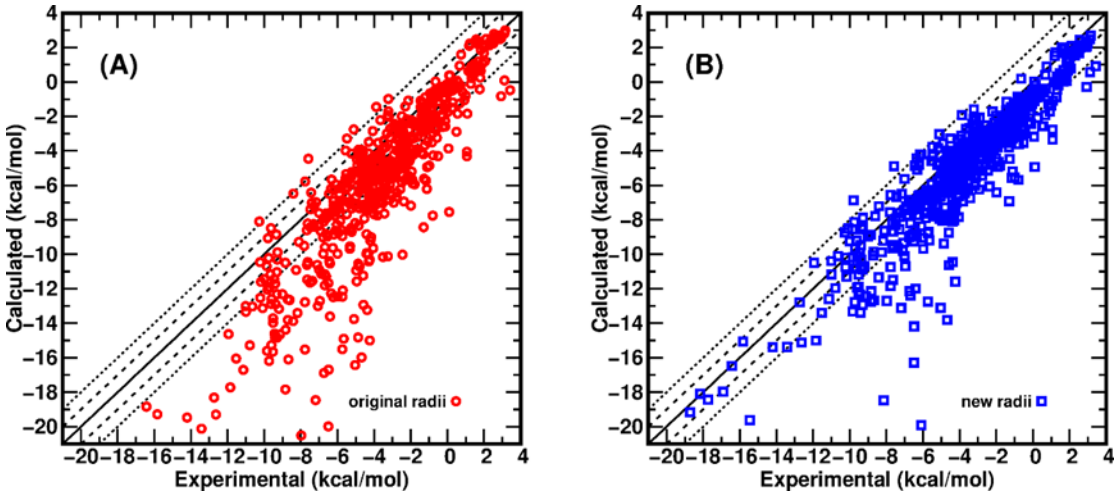

Figure 5 Comparison between experimental SFE and calculated SFE using ABCG2 with original and new radii for all molecules

A, The experiment SFE of all molecules vs the calculated SFE with ABCG2 and original radii (red circles). B, The experiment SFE of all molecules vs the calculated SFE with ABCG2 and updated radii (blue squares). The

lines are eye-guided lines for ideal matching of calculation vs. experiment (solid line), with error of ±1 kcal/mol (dashed line), and with error of ±2 kcal/mol (dotted line), respectively.

3.5 The Performance of MMPBSA Calculation Using New Radii Parameters & Nonpolar SFE model and RESP & AM1-BCC charge

The updated PB radii parameters and new nonpolar SFE model were applied in the calculation of SFE using MM-PBSA and RESP or AM1-BCC charge model. It was exciting that the performance of MM-PBSA calculation using other charge model also improved as **Figure 6** and **Figure 7** demonstrated. The detailed results of MM-PBSA for training set molecules (excluding molecules with multiple functional groups) with AM1-BCC and RESP charge model before radii optimization is shown in **Table S2**, **S4**, respectively. After the radii optimization, the detailed results of MM-PBSA for training set molecules (excluding molecules with multiple functional groups) with AM1-BCC and RESP charge model is shown in **Table S3**, **S5**, respectively. The comparison is shown in **Figure S2**, **S3**, **S4**, **S5**. We can observe that the magnitudes of MSE, MUE, and RMSE of different functional group molecules usually decrease from the results of original atom radii (in red color) to those of updated atom radii (in blue color) and the overall performance became more balanced for different functional groups. Although for some functional groups, minor increase in error were observed.

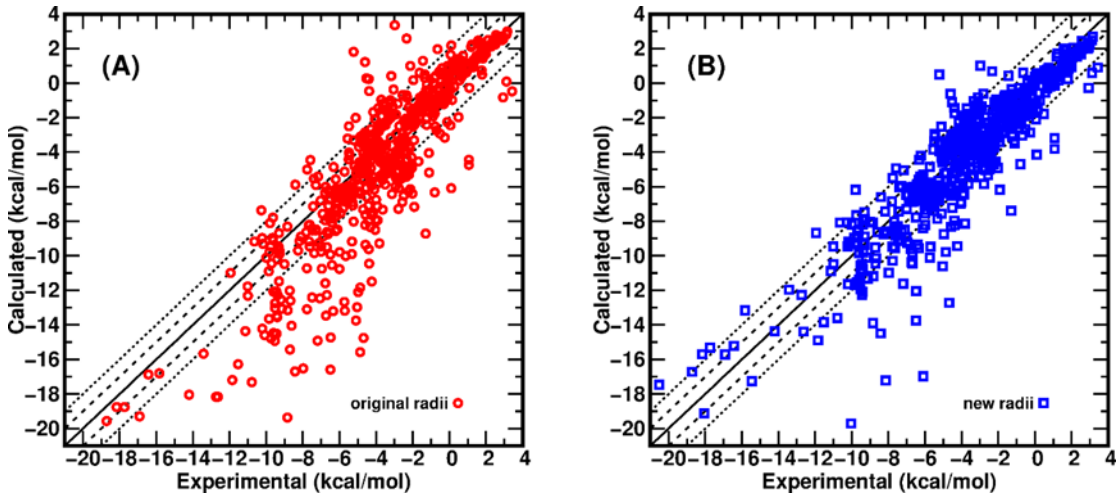

Figure 6 Comparison between experimental SFE and calculated SFE using AM1-BCC with original and new radii

A, The experiment SFE of small molecule vs the calculated SFE with AM1-BCC and original radii. B, The experiment SFE of small molecule vs the calculated SFE with AM1-BCC and updated radii. The color scheme is the same as Figure 2.

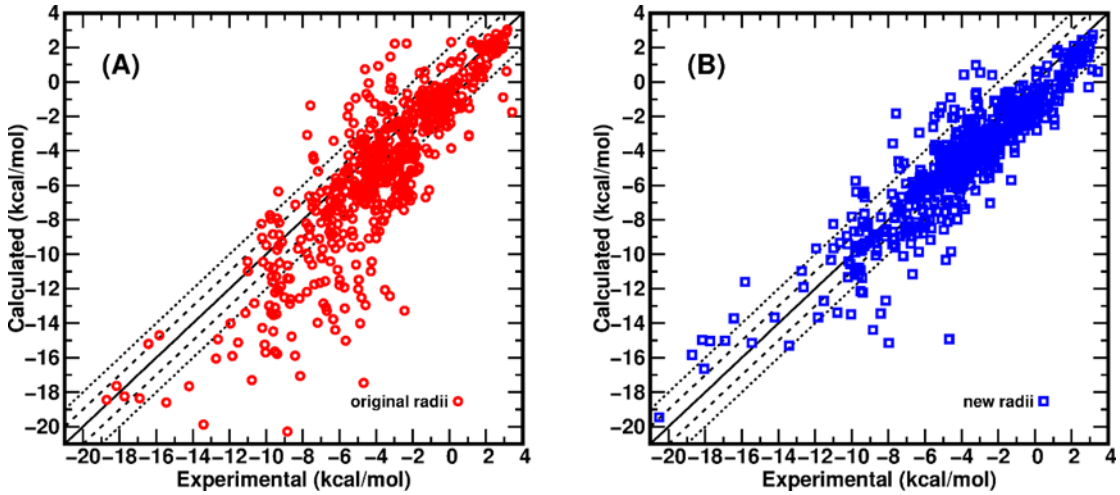

Figure 7 Comparison between experimental SFE and calculated SFE using RESP with original and new radii

A, The experiment SFE of small molecule vs the calculated SFE with RESP and original radii. B, The experiment SFE of small molecule vs the calculated SFE with RESP and updated radii. The color scheme is the same as Figure 2.

As **Figure S2** indicates, for MM-PBSA calculation using AM1-BCC charge, the performance of sulfone, phosphoryl and esters improved greatly, while for amides, hydrocarbon +

iodide and aromatic hydrocarbon molecules, the prediction errors increased slightly. The overall performance for 544 molecules was improved, the MSE increased a little bit from -0.57 kcal/mol to 0.73 kcal/mol, the MUE decreased to 1.22 kcal/mol from 1.37 kcal/mol, the RMSE decreased to 1.62 kcal/mol from 2.00 kcal/mol.

The improvement was even greater for MM-PBSA calculation using RESP charge. The systematic error for calculation of amides, nitrile, hydrocarbon + iodide functional group series increased a little bit. While dramatic improvement was observed for sulfone, phosphoryl, nitro and nitro-oxy functional groups. The RMSE of sulfone functional group decreased from 5.84 kcal/mol to 2.19 kcal/mol. The RMSE of phosphoryl functional group decreased from 3.68 kcal/mol to 0.43 kcal/mol. For nitro and nitrooxy functional groups, the RMSE changed from 4.10 kcal/mol and 5.27 kcal/mol to 1.28 kcal/mol and 2.03 kcal/mol, respectively. The overall MSE decreased from the previous -1.05 kcal/mol to 0.43 kcal/mol, the MUE decreased from 1.70 kcal/mol to 1.09 kcal/mol, the RMSE decreased to 1.53 kcal/mol from the previous 2.34 kcal/mol.

3.6 The Performance of Adopting New PB Radii Parameters and Nonpolar SFE Model for MMPBSA Calculation to Predict the Binding Free Energy

As mentioned before, the four drug targets used in this study is the most difficult ones among the eight extensively studied drug targets to evaluate the performance of new free energy calculation methods[49-51]. According to a paper published by our lab[51], the Pearson's correlation of absolute binding free energy between MM-PBSA-WSAS calculation results and experiment values for BACE1, JNK1, P38, PTP1B are 0.29, 0.04, 0.22, -0.25, respectively.

After the new charge model and nonpolar SFE model adopted, the new calculation result is shown in **Table 4** and **Figure 8**. Except for JNK1, which the RMSE for direct calculation increased, all the other systems have improved performance for correlation and absolute binding free energy.

Table 4 Binding free energy prediciton for 4 systems

The correlation and RMSE between experiment binding free energy and MM-PBSA calculated binding free energy for 4 protein ligand systems.

			Old Parameters			New Parameters		
System	Number of Ligands	Inner Dielectric	R	RMSE (after regression)	RMSE (direct calculation)	R	RMSE (after regression)	RMSE (direct calculation)
BACE1	41	1	0.28	1.05	4.53	0.49	1.44	2.30
JNK1	21	1	0	1.88	2.04	0.28	1.15	6.46
P38	35	1	0.08	3.65	4.28	0.19	2.61	2.71
PTP1B	27	4	0.52	1.12	24.78	0.55	1.19	17.92

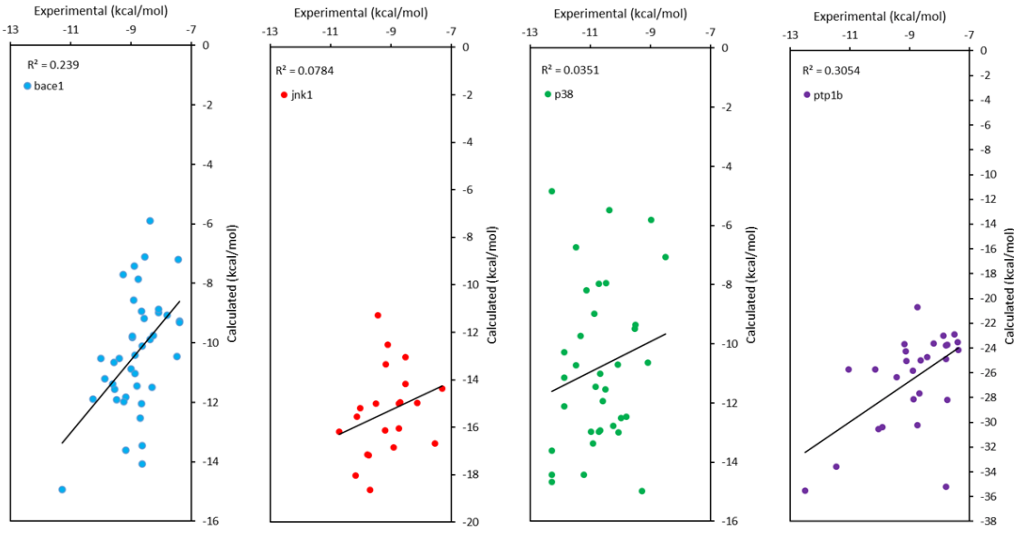

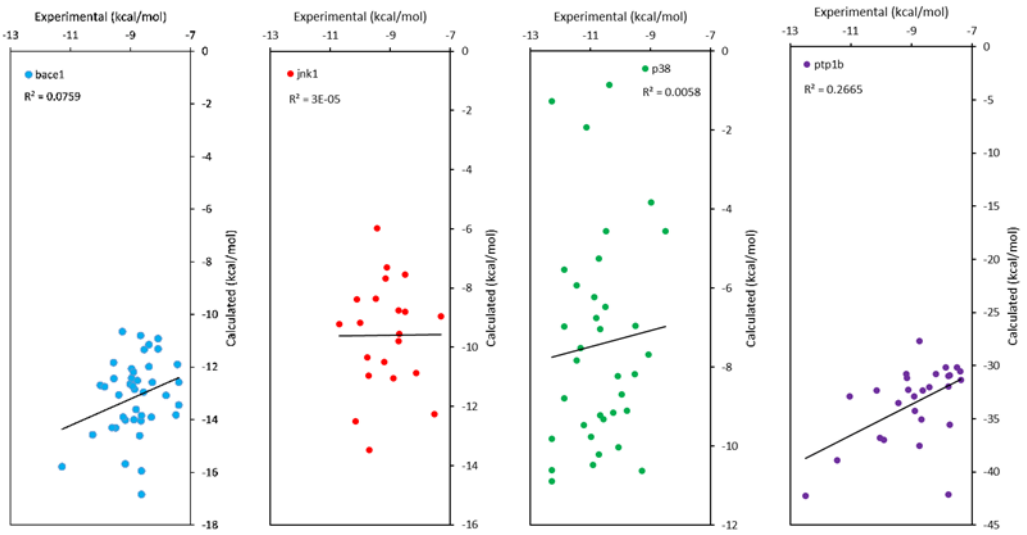

Figure 8 Absoulte binding free energy prediction for 4 systems before and after radii optimization

Absolute binding free energy prediction by MM-PBSA method versus experiment binding free energy for four protein ligand systems. The calculation using new parameters are on the top and the calculation using old parameters are on the bottom.

3.7 The Performance of New PB Radii Combined with New Nonpolar Model on Octanol SFE Prediction

After conducting PB calculation with the octanol dielectric constant and the optimized PB radii from the previous steps, the deviation between experiment and PB results (represent the nonpolar part of solvation free energy) was obtained. Then the new nonpolar model for octanol SFE calculation was established based on the surface area of the solute molecule. This was done by fitting the MSSAS against experiment SFE minus PB results. We only got 238 molecules (9 out of 247 has error when calculation MM-PBSA) in our training set molecules. To get a better model, we build the model based on all the data we have. Before doing that, a 10-fold cross validation was conducted for 1000 rounds to minimize the bias of the model. The data was

randomly divided into 10 groups and each time 9 out of 10 groups of data were used as training set and the 1 group of data left was used as test set. The mean MSE was 1.76 for the total 1000 rounds. The nonpolar model was then built by the regression between experiment SFE minus PB, and MSSAS. After the model was established, we calculated the SFE based on the model and compared it with experimental SFE. Five molecules stood out as they had relatively large (cutoff value = 5 kcal/mol) deviation between experiment and calculated SFE. So, we eliminated those outliers and redo the regression. The final model we got for octanol SFE estimation was as **Equation 7** shows:

$$SFE_{octanol} = PB - 0.012 * MSSAS + 2.82$$

Equation 7 Nonpolar model for SFE calculation in octanol

3.8 The Performance logP Prediction for Training Set

As aforementioned, in the thermodynamic point of view, the logarithm of partition coefficient (logP) can be estimated by the SFE in octanol and water. Since our SFE calculation model was trained based on the SFE of training set molecules, it is not surprising that our model performs quite well for the training set molecules. There are in total 633 water SFE data and 238 octanol SFE data, and we got 171 experimental logP data. Together, there are 156 common molecules which has both water and octanol SFE and experimental logP, and for these molecules our logP prediction can reach a RMSE of 0.92.

3.9 The Performance of logP Prediction for ZINC Dataset

To validate our newly proposed logP model, the logP prediction accuracy was tested on 470 molecules form ZINC database [74]. ZINC database is a drug like database which comprise of tens of millions of purchasable compounds. In our validation set, the molecules from ZINC database are distributed between molecule weight from 160 to 600 Da. For the molecules in ZINC database, the RMSE of our prediction compared to the experimental value is 0.91, which is better than the commonly used program Open Babel [75], and also outperform the commercial software like Maestro and Sybyl. The detailed comparison for the logP prediction accuracy for the molecules in ZINC dataset are listed in **Table 5**. The prediction results are in **Figure 9**.

Table 5 logP prediction for ZINC molecules using our method and three commonly used programs

The comparison of logP prediction accuracy for ZINC molecules using our mixed model and three commonly used programs (Open Babel, Maestro, Sybyl). Note: For QikProp in Maestro, 3 out of 503 molecules did not yielded results.

	Our method	Open Babel	Maestro	Sybyl
RMSE	0.91	1.13	1.25	1.68

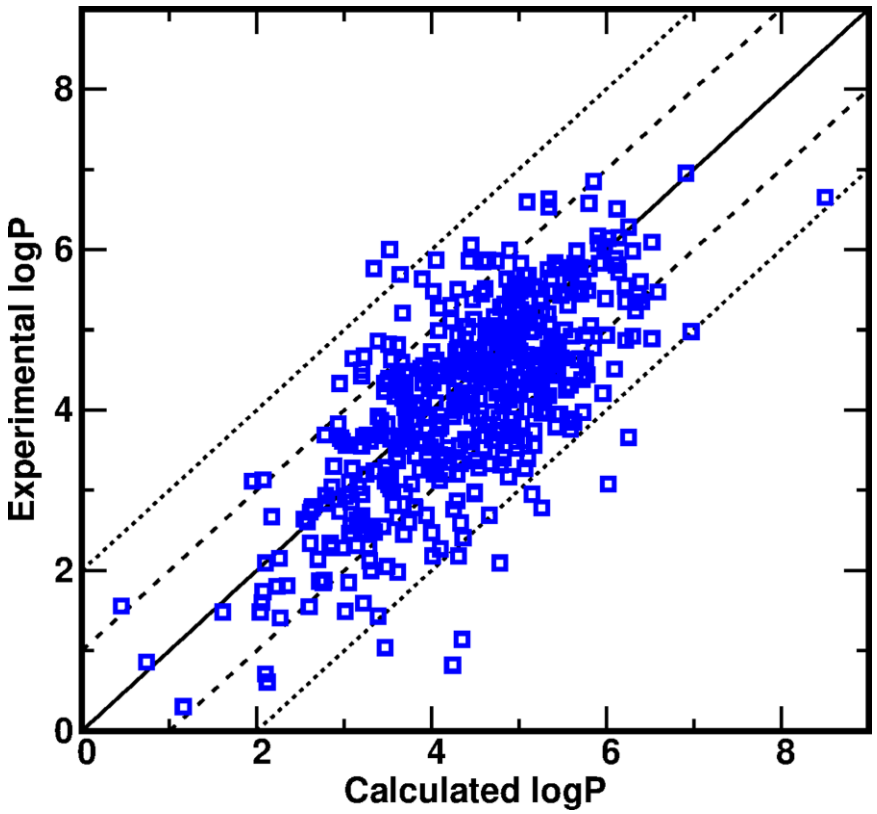

Figure 9 Calculated logP vs. experimental logP for ZINC molecules

4.0 DISCUSSION

As aforementioned, various methods ranging from simple empirical statistical methods like QSPR to complex alchemical perturbation methods like FEP/TI are used to estimate the solvation free energy. Some QSPR model can achieve relatively good accuracy, for example, the hybrid QSPR model proposed by Borhani et al.[76]. In total 1777 experimental SFE data of 295 solutes in 210 solvents were obtained. The model was built based on the 1421 training SFE data and yielded a RMSE of 0.52 kcal/mol for 356 test set SFE data. But it is hard to interpret the model physically and the good performance tends to be limited in the molecules which are similar to the training set. Alchemical methods are computational demanding but usually yield better results. Nevertheless, most of the earlier SFE prediction efforts using alchemical calculation still got relatively large systematic error. The model using OPLS_2005[77] force field had a RMSE of 1.33 kcal/mol in HFE prediction of 239 solutes.

Mobley et al. tested the performance of SFE prediction of 17 compounds using MM-PBSA with AM1-BCC charge and their ZAP-9 radii set[78]. The solvent structures were optimized by Gaussian 03[79] at the B3LYP/6-31G** level of theory. Then charge was obtained using OpenEye implementation of AM1-BCC v1[20, 21]. The MM-PBSA was calculated using OpenEye's PB solver ZAP v2.0[80]. The RMSE for PB compared to the test set was 1.87 ± 0.03 kcal/mol[78], which agrees with our MM-PBSA calculation before parameter adjustment.

Based on our observations, when it comes to the HFE calculation, ABCG2 and AM1-BCC outperform RESP charge in many aspects. The GAFF2 force field was developed using RESP charge model and TIP3P water model[22]. The original aim of AM1-BCC charge was to produce atomic charges that emulate the HF/6-31G* electrostatic potential (ESP) quickly and efficiently to

serve as a robust alternative to RESP charge. The parameterization of BCCs was performed by fitting to the HF/6-31G* ESP of a training set with more than 2700 molecules. However, some atom types with large errors of relative SFE calculations (nitrogen in amine and nitro function groups) were tuned to make the calculation results accord with the experiment value[20]. The validation of the AM1-BCC charge compared the experimental SFE of diverse set of 40 molecules with calculated SFE using alchemical method with AM1-BCC charge model, the MUE was within 0.69 kcal/mol[20]. Meanwhile, the MUE of calculated SFE with RESP charge model on the same set is 1.36 kcal/mol[20]. Since AM1-BCC perform better than RESP on SFE calculation by alchemical methods, it is reasonable that AM1-BCC charge and AM1-BCC based ABCG2 charge show better performance on small molecule HFE prediction by MM-PB/GBSA than RESP as demonstrated in our validation.

ABCG2 charge are newly developed charge model based on AM1-BCC scheme which is compatible with GAFF2 force field. It was specially optimized using the thermodynamic integration (TI) calculation of a smaller set of 441 HFE data. We found that when calculating the HFE using MM-PBSA method, the systemic error increased compared to TI calculation. The reported MSE and MUE using TI calculation are 0.65 kcal/mol and 1.03 kcal/mol respectively[22]. While the MSE and MUE using PBSA are generally larger. Although ABCG2 charge are optimized using partial of the HFE data used in this study, its performance of HFE prediction using PB method are not the best among the three charge models. This is due to the fact that the radii parameters used for PB calculation are Parse radii[81] which not compatible with the new ABCG2 charge. With our newly derived atom radii parameters, users can expect better results when conducting PB calculation with ABCG2 charge.

From theoretical perspective, MM-PBSA should have better accuracy and MM-GBSA should be less computational demanding. But as a matter of fact, the accuracy of the method depends on the system being studied. For the estimation of HFE, PB calculation yielded worse results with RESP and ABCG2 charge models, while PB and GB are comparable when using AM1-BCC charge to do the HFE prediction (**Table 1**). The detailed results of HFE prediction after the adjustment of atom radii is listed in **Table 6**.

Table 6 The SFE prediction using three charge models after radii optimization

After the radii optimization, the performance of RESP, AM1-BCC and ABCG2 charge model with PBDELPHI and new nonpolar model on SFE prediction for 544 molecules. The unit of MSE, MUE and RMSE is kcal/mol.

	RESP charge					AM1-BCC charge					ABCG2 charge				
Calculation method	MSE	MUE	RMSE	PI	R	MSE	MUE	RMSE	PI	R	MSE	MUE	RMSE	PI	R
PBDELPHI	0.43	1.09	1.53	0.90	0.90	0.73	1.22	1.62	0.91	0.91	0.00	0.75	1.05	0.95	0.95

In order to make our radii parameter set useful for free energy calculation involving protein systems, we incorporated 18 charged molecules which serve as model molecules for amino acids. The charged molecules can be divided into three groups: ammonium, carboxylate and arginine which represent the commonly encountered charged functional groups in protein. The experiment HFE data of these molecules are from the MNsolv database[82]. As **Table 7** shows, before the radii optimization, the performance of MM-PBSA using ABCG2 charge is good for arginine, but the error is large for other charge molecules. So, we kept the radii for arginine the same and tuned the oxygen for carboxylates and hydrogen atoms in ammonium. The atom type of oxygen for carboxylates and hydrogens for primary, secondary and tertiary amine are all newly defined. Here we did not tune the nitrogen radii to improve ammonium performance because that the nitrogen is in the inner layer of the functional group, so when its radii changed, the calculation results almost

remained the same. The results after radii optimization are listed as **Table 8**. We can see that after adopting the updated radii. The MSE, MUE and RMSE improved significantly.

Table 7 SFE calculation for charged molecules before radii optimization

The performance of MM-PBSA (PB_DELPHI) using ABCG2 charge model for charge molecules before atom radii optimization. The unit of MSE, MUE and RMSE is kcal/mol.

Subclass	Number	MSE	MUE	RMSE	PI	R	k	b
Tertiary-ammoniums	3	4.61	4.61	4.75	1	1	1.27	20.2
Secondary-ammoniums	6	5.55	5.55	5.68	0.97	0.97	1.33	27.22
Primary-ammoniums	5	3.57	3.57	3.86	0.93	0.96	1.26	22.55
Carboxylates	3	-2.76	2.76	2.8	1	1	1.41	29.07
Arginine	1	-0.11	0.11	0.11	NA	NA	NA	NA

Table 8 SFE calculation for charged molecules after radii optimization

The performance of MM-PBSA (PB_DELPHI) using ABCG2 charge model for charged molecules after atom radii optimization. The unit of MSE, MUE and RMSE is kcal/mol.

Subclass	Number	MSE	MUE	RMSE	PI	R	k	b
Tertiary-ammoniums	3	1.6	1.9	2.25	1	1	1.38	23.14
Secondary-ammoniums	6	1.54	2.03	2.09	0.97	0.97	1.42	29.11
Primary-ammoniums	5	0.9	1.25	1.81	0.93	0.96	1.31	23.34
Carboxylates	3	0.32	0.46	0.57	1	1	1.38	29.91
Arginine	1	-0.11	0.11	0.11	NA	NA	NA	NA

The accurate prediction of logP is an important topic in molecular modeling and computer aided drug design. A full spectrum of calculation methods has been adopted in logP prediction, ranging from the fast QSPR method to time consuming high level alchemical methods.

Our logP prediction is a mixed model which is physical based and adopted empirical corrections, thus theoretically more rigorous than QSPR method and faster than alchemical method.

In theory, the nonpolar part of SFE is related to cavity, dispersion and solvent structure free energy in the process of solvation, while most methods estimation nonpolar part using solvent

accessible surface area (SASA). In order to improve the accuracy of SFE prediction, we took both cavity formation and Van der Walls interaction into account when calculating the nonpolar SFE term. The new nonpolar HFE model was generated by fitting the nonpolar HFE with WSAS (weighted solvent accessible surface area) which correspond to the cavity formation of the solvation process and MSSAS which correspond to the Van der Walls interaction (dispersion term) in the solvation process. When calculating MSSAS, the weight applied to each atom type was calculated by Lennard Jones potential[83-85]. We compare the performance when calculating the nonpolar SFE with both MSSAS, WSAS and MSSAS alone, the result shows that the prediction accuracy is quite similar. Finally, we decide to only keep MSSAS when calculate nonpolar SFE as it demonstrates comparable accuracy to taking both MSSAS and WSAS into account, and it is similar to previous nonpolar model.

5.0 CONCLUSION

In this study, the influence of applying the newly developed ABCG2 charge model on the calculation by MM-PB/GBSA was explored and compared to AM1-BCC and RESP charge models. We found that both ABCG2 and AM1-BCC charge has its own advantage towards SFE prediction. For MM-PBSA calculation using ABCG2 charge model, new PB radii parameter set was also obtained by iterative calculation and adjustment. And a new nonpolar SFE model was generated accordingly. The new PB radii combined with the nonpolar SFE model dramatically improved the HFE calculation performance. The RMSE of 544 molecules decreased from 3.39 kcal/mol to 2.09 kcal/mol. The versatility of the new parameter set was further validated by applying to the calculation of HFE using RESP and AM1-BCC charge. Finally, the charge model and the new nonpolar SFE model were tested on BACE1, JNK1, P38, PTP1B and improved the prediction accuracy for protein ligand binding free energy using MM-PBSA method. Our results indicated that this newly derived PB radii parameter has the potential to improve the HFE calculation and protein ligand binding free energy prediction using MM-PBSA method universally.

The past decades have witnessed the dramatic improvement of the computer hardware and accelerated computational speed. Consequently, accurate but not very computational demanding methods might gain more popularity as computational resources becoming more approachable. We proposed a new approach to calculate logP of drug like molecules in an accurate and computationally feasible way. The logP calculation is based on physical point of view which takes the SFE of molecule in water and octanol as input and further modified by empirical corrections. With that, we were able to achieve high accuracy (RMSE = 0.92) for drug molecules in ZINC database which outperform other commonly used logP prediction methods.

Appendix A Supplementary Figures

Appendices contain supplementary or illustrative material or explanatory data too lengthy to be included in the text or not immediately essential to the reader's understanding of the text.

When using the Appendix Style, type the title of the Appendix section after the inserted heading.

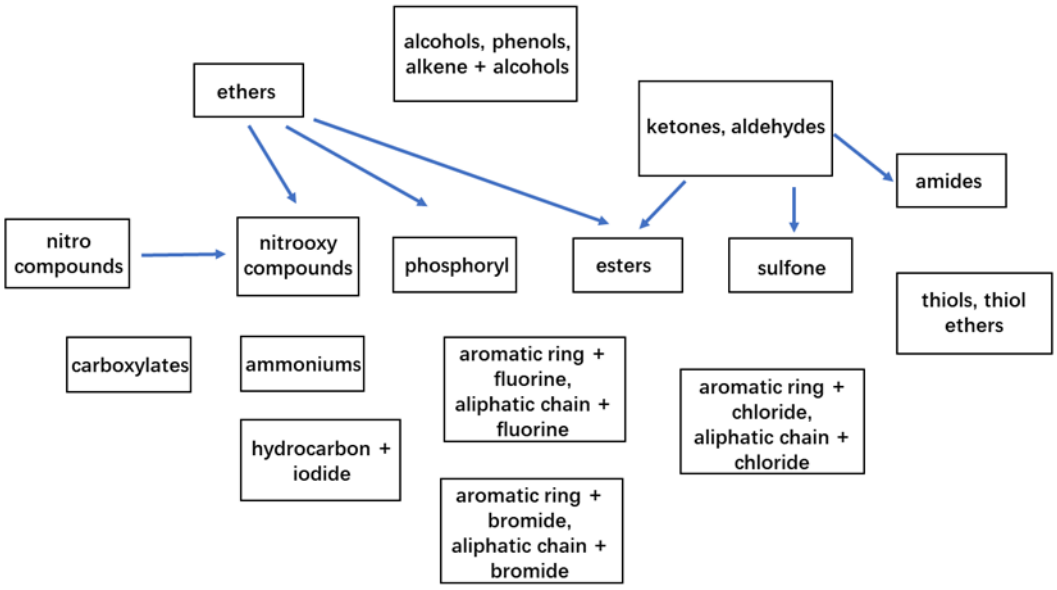

Figure S1 The scheme for PB radii parameter adjustment of different functional groups

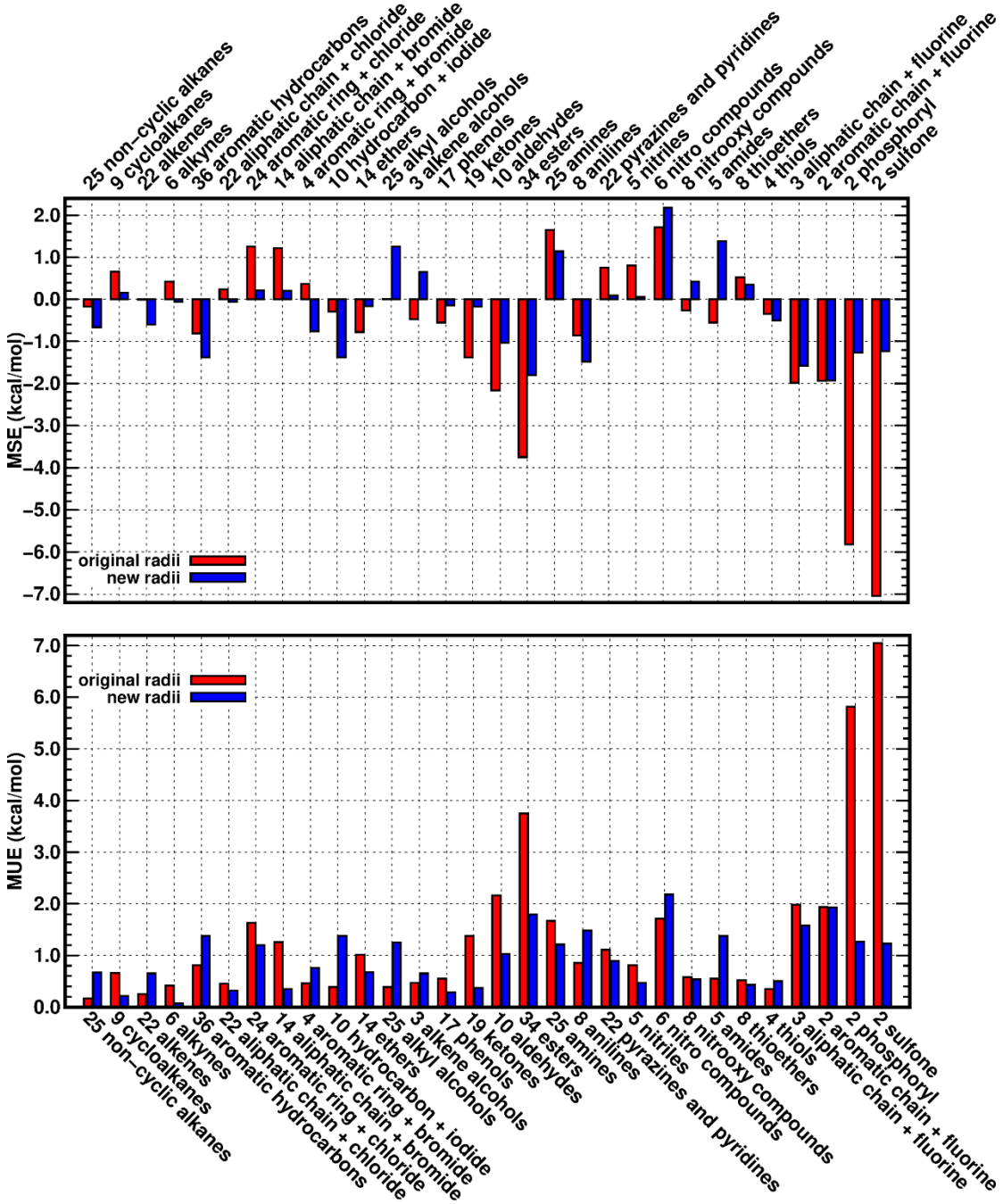
25 non−cyclic alkanes
9 cycloalkanes
22 alkenes
6 alkynes
36 aromatic hydrocarbons
22 aliphatic chain + chloride
24 aromatic chain + chloride
14 aliphatic chain + bromide
4 aromatic ring + bromide
10 hydrocarbon + iodide
14 ethers
25 alkyl alcohols
3 alkene alcohols
17 phenols
19 ketones
10 aldehydes
34 esters
25 amines
8 anilines
22 pyrazines and pyridines
5 nitriles
6 nitro compounds
8 nitrooxy compounds
5 amides
8 thioethers
4 thiols
3 aliphatic chain + fluorine
2 aromatic chain + fluorine
2 phosphoryl
2 sulfone
MSE (kcal/mol)
original radii
new radii
MUE (kcal/mol)
original radii
new radii

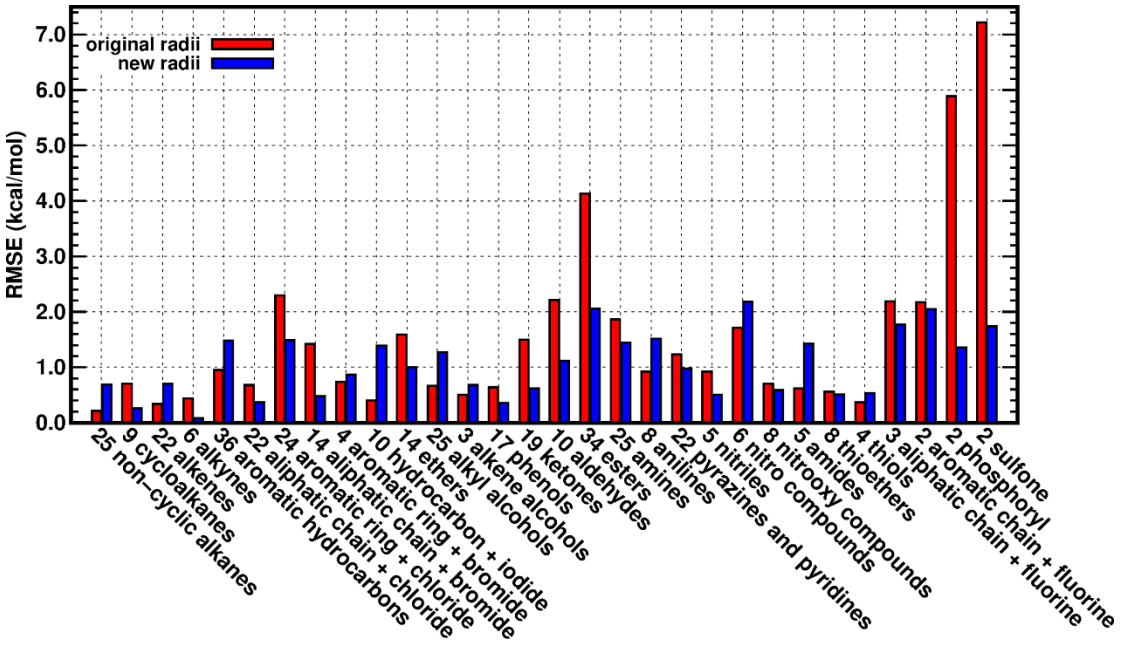

Figure S2 Comparisong of SFE calculation using AM1-BCC charge before and after radii optimization

The comparison of MSE, MUE and RMSE of SFE calculation for training set molecules (excluding molecules with multiple functional groups) using AM1-BCC charge before and after adjustment of atom radii. The results from original PB atom radii are in red color, and the results from updated PB atom radii are in blue color.

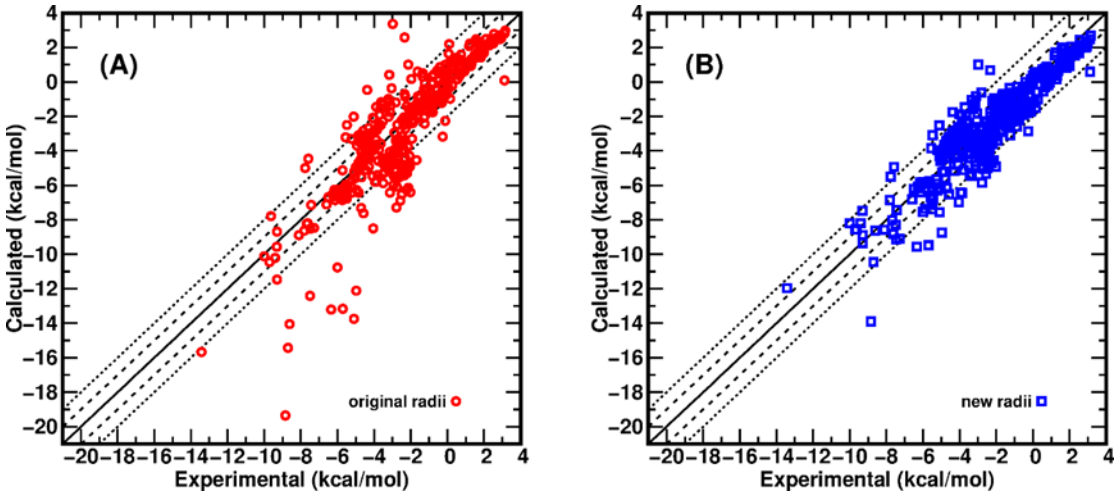

Figure S3 Comparison between experimental SFE and calculated SFE using AM1-BCC with original and new radii

A, The experiment SFE of training set molecules (excluding molecules with multiple functional groups) vs the calculated SFE with AM1-BCC charge and original radii (red circles). B, The experiment SFE of training set molecules (excluding molecules with multiple functional groups) vs the calculated SFE with AM1-BCC and updated radii (blue squares). The lines are eye-guided lines for ideal matching of calculation vs. experiment (solid line), with error of ±1 kcal/mol (dashed line), and with error of ±2 kcal/mol (dotted line), respectively.

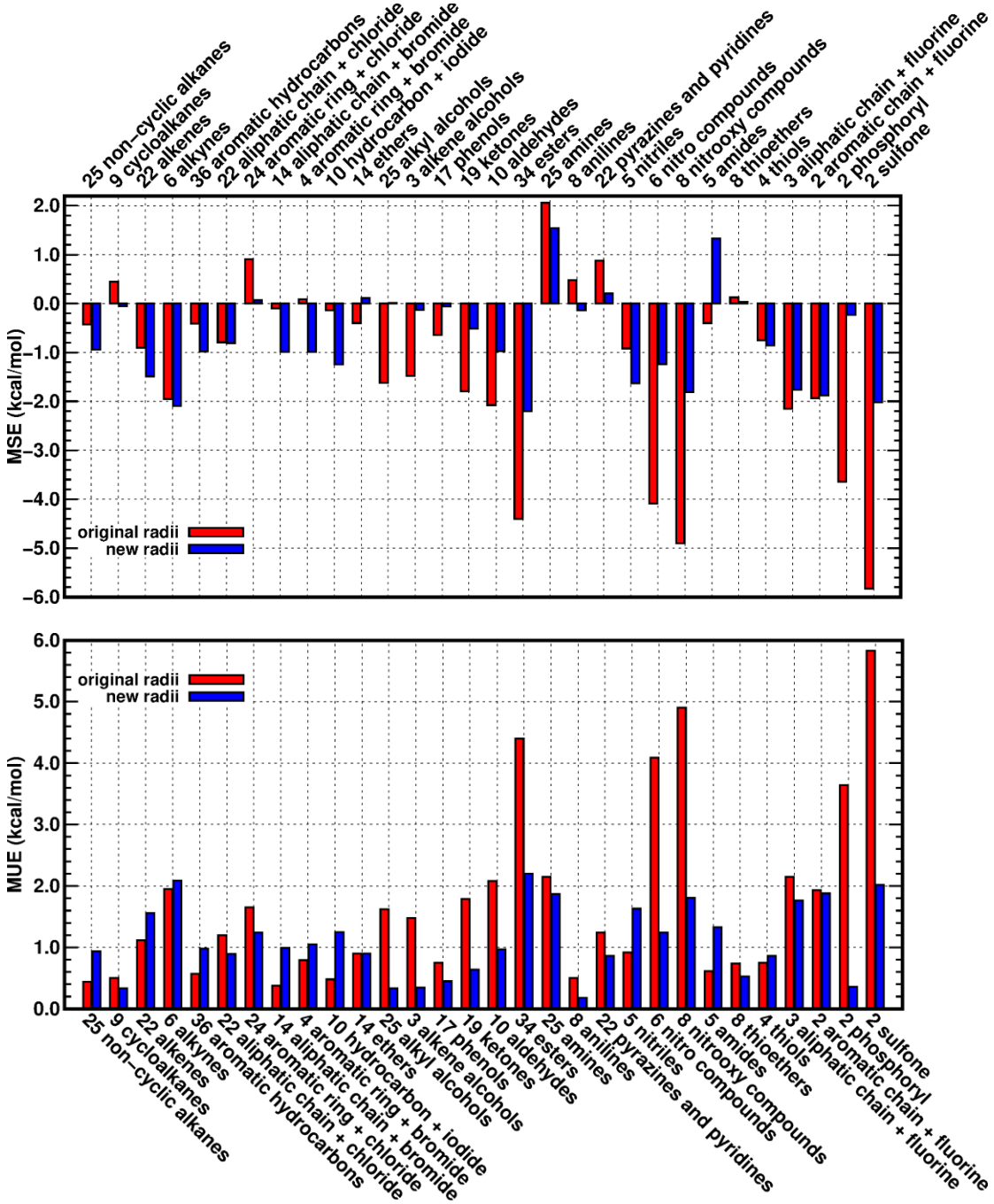

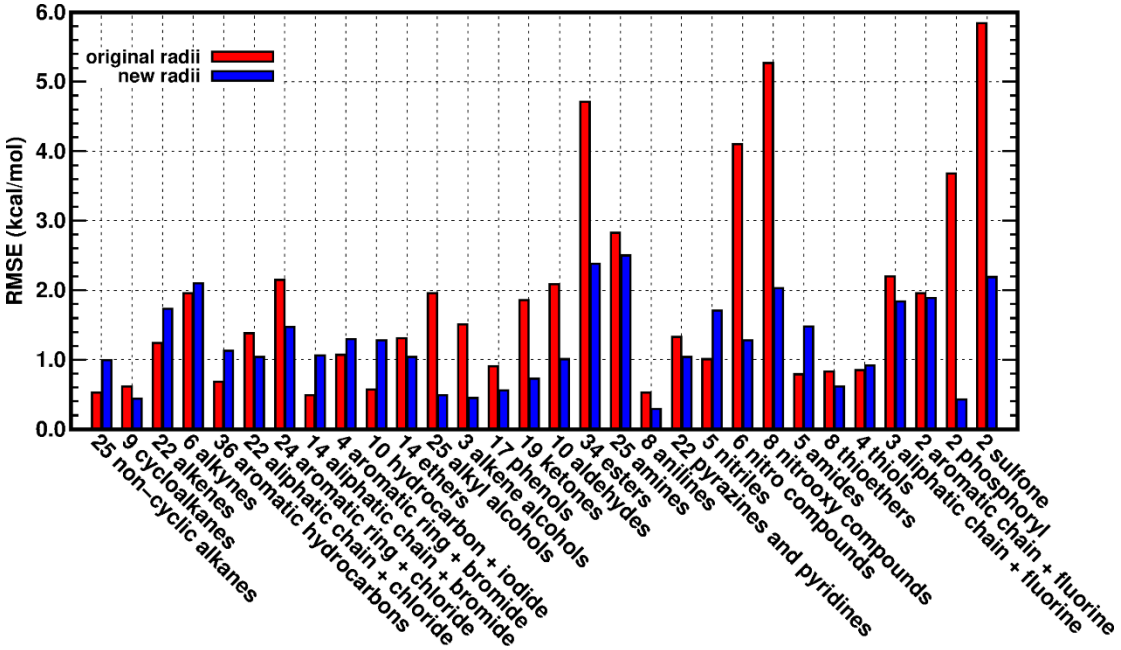

Figure S4 Comparisong of SFE calculation using RESP charge before and after radii optimization

The comparison of MSE, MUE and RMSE of SFE calculation for training set molecules (excluding molecules with multiple functional groups) using RESP charge before and after adjustment of atom radii. The results from original PB atom radii are in red color, and the results from updated PB atom radii are in blue color.

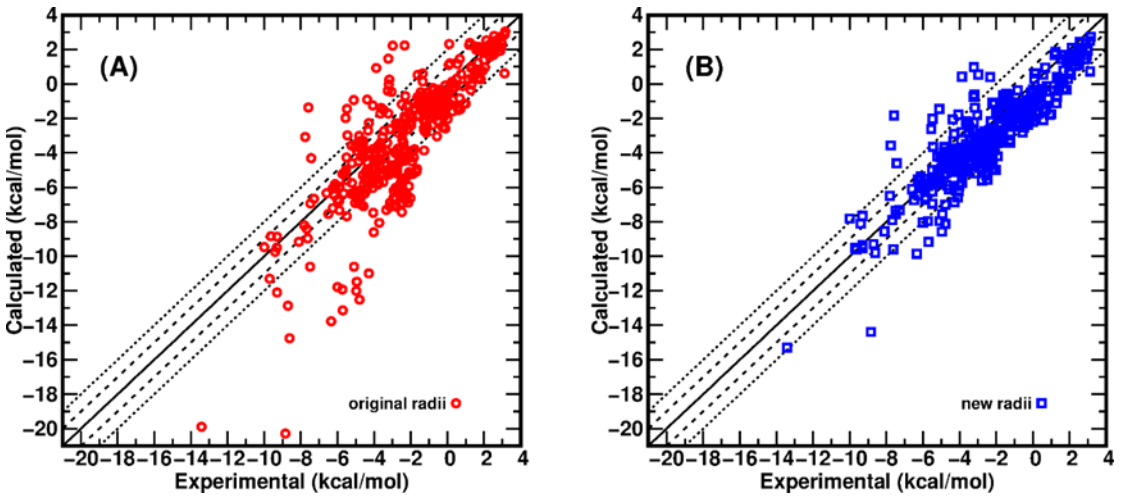

Figure S5 Comparison between experimental SFE and calculated SFE using RESP with original and new radii

A, The experiment SFE of training set molecules (excluding molecules with multiple functional groups) vs the calculated SFE with RESP charge and original radii (red circles). B, The experiment SFE of training set

molecules (excluding molecules with multiple functional groups) vs the calculated SFE with RESP and updated radii (blue squares). The lines are eye-guided lines for ideal matching of calculation vs. experiment (solid line), with error of ±1 kcal/mol (dashed line), and with error of ±2 kcal/mol (dotted line), respectively.

Appendix B Tables

Table S1 The atom type for different functional groups.

Functional Group	Atom Type 1	Atom Type 2
Alkynes	***c1***	
Aliphatic chain + chloride	***cl***	
Aromatic ring + chloride	***cl***	
Aliphatic chain + bromide	***br***	
Aromatic ring + bromide	***br***	
Hydrocarbon + iodide	***i***	
Ethers	***os***	
Alkyl alcohols	***oh***	
Alkene + alcohols	***oh***	
Phenols	***oh***	
Ketones	***o***	
Aldehydes	***o***	
Esters	***o***	***os***
Nitriles	***c1***	
Nitro compounds	***o*** **(newly defined as** ***on*****)**	
Nitrooxy compounds	***o*** **(newly defined as** ***on*****)**	***os***
Amides	***o***	
Thioethers	***ss***	
Thiols	***sh***	
Aliphatic chain + fluorine	***f***	
Aromatic ring + fluorine	***f***	
Phosphoryl	***p5***	***os***
Sulfone	***s6***	***o***
Primary-ammoniums	***hn*** **(newly defined as** ***hn1*****)**	
Secondary-ammoniums	***hn*** **(newly defined as** ***hn2*****)**	
Tertiary-ammoniums	***hn*** **(newly defined as** ***hn3*****)**	
Carboxylates	***o*** **(newly defined as** ***oi*****)**	

Table S2 The performance of MM-PBSA (PB_DELPHI) using AM1-BCC charge model before atom radii optimization for training set molecules

Training set molecules excludes molecules with multiple functional groups. The unit of MSE, MUE and RMSE is kcal/mol.

Subclass	Number	MSE	MUE	RMSE	PI	R	k	b
Non-cyclic alkanes	25	-0.17	0.17	0.21	0.96	0.94	0.76	0.46
Cycloalkanes	9	0.66	0.66	0.71	0.96	0.93	0.56	1.38
Alkenes	22	-0.01	0.25	0.34	0.81	0.76	0.68	0.37
Alkynes	6	0.42	0.42	0.44	1	0.99	0.74	0.47

Aromatic hydrocarbons	36	-0.81	0.81	0.95	0.96	0.97	1.25	-0.42
Aliphatic chain + chloride	22	0.24	0.45	0.68	0.9	0.86	1.25	0.43
Aromatic ring + chloride	24	1.25	1.63	2.3	0.01	-0.03	-0.05	-0.91
Aliphatic chain + bromide	14	1.22	1.26	1.42	0.62	0.67	0.36	0.87
Aromatic ring + bromide	4	0.37	0.46	0.74	0.08	0.33	0.45	-0.68
Hydrocarbon + iodide	10	-0.29	0.39	0.4	1	0.98	0.7	-0.5
Ethers	14	-0.78	1.01	1.59	0.93	0.91	1.81	1.11
Alkyl alcohols	25	0.01	0.39	0.67	0.99	1	1.31	1.51
Alkene + alcohols	3	-0.47	0.47	0.5	0.43	0.74	0.71	-1.84
Phenols	17	-0.55	0.55	0.64	0.81	0.9	0.9	-1.18
Ketones	19	-1.38	1.38	1.5	0.87	0.88	1.38	-0.15
Aldehydes	10	-2.16	2.16	2.21	0.77	0.64	0.84	-2.62
Esters	34	-3.75	3.75	4.13	0.9	0.97	2.03	-0.61
Amines	25	1.65	1.67	1.86	0.85	0.87	0.97	1.53
Anilines	8	-0.86	0.86	0.92	0.99	0.97	1	-0.87
Pyrazines and pyridines	22	0.75	1.11	1.23	0.91	0.8	1.04	0.95
Nitriles	5	0.81	0.81	0.92	1	0.96	2.98	8.31
Nitro compounds	6	1.71	1.71	1.72	0.95	0.92	0.73	0.81
Nitrooxy compounds	8	-0.26	0.58	0.71	0.98	0.99	1.38	1.03
Amides	5	-0.55	0.55	0.62	0.81	0.92	0.79	-2.48
Thioethers	8	0.52	0.52	0.56	0.95	0.95	1.29	0.99
Thiols	4	-0.35	0.35	0.37	0.82	0.92	2.13	0.9
Aliphatic chain + fluorine	3	-1.98	1.98	2.19	0.97	0.82	0.51	-1.52
Aromatic ring + fluorine	2	-1.94	1.94	2.17	-1	-1	-2.55	-3.8
Phosphoryl	2	-5.82	5.82	5.89	1	1	2.51	6.45
Sulfone	2	-7.05	7.05	7.22	1	1	0.09	-13.28
Sum	394	-0.36	1.18	1.81	0.88	0.86	1.09	-0.14

Table S3 The performance of MM-PBSA (PB_DELPHI) using AM1-BCC charge model after atom radii optimization

Training set molecules excludes molecules with multiple functional groups. The unit of MSE, MUE and RMSE is kcal/mol

Subclass	Number	MSE	MUE	RMSE	PI	R	k	b
Non-cyclic alkanes	25	-0.67	0.67	0.69	0.96	0.93	1	-0.68
Cycloalkanes	9	0.16	0.21	0.26	0.96	0.93	0.73	0.61
Alkenes	22	-0.6	0.65	0.71	0.76	0.73	0.76	-0.31
Alkynes	6	-0.06	0.07	0.08	1	0.99	0.94	-0.05
Aromatic hydrocarbons	36	-1.38	1.38	1.48	0.96	0.97	1.27	-0.95
Aliphatic chain + chloride	22	-0.06	0.32	0.37	0.93	0.92	1.09	0.01
Aromatic ring + chloride	24	0.21	1.2	1.49	0.16	0.09	0.12	-1.61
Aliphatic chain + bromide	14	0.2	0.35	0.48	0.9	0.9	0.69	0.03
Aromatic ring + bromide	4	-0.76	0.76	0.87	0.56	0.59	0.62	-1.46
Hydrocarbon + iodide	10	-1.38	1.38	1.39	1	0.98	1.07	-1.33
Ethers	14	-0.16	0.68	1	0.93	0.91	1.49	0.97
Alkyl alcohols	25	1.25	1.25	1.27	0.99	0.99	1.03	1.38
Alkene + alcohols	3	0.65	0.65	0.68	0.43	0.8	1.13	1.25
Phenols	17	-0.14	0.29	0.36	0.77	0.9	0.96	-0.37
Ketones	19	-0.17	0.37	0.62	0.91	0.9	1.45	1.3
Aldehydes	10	-1.03	1.03	1.12	0.77	0.71	1.02	-0.98
Esters	34	-1.8	1.8	2.06	0.9	0.95	1.48	-0.34
Amines	25	1.14	1.21	1.44	0.85	0.87	0.98	1.05
Anilines	8	-1.48	1.48	1.51	0.99	0.97	1.01	-1.4
Pyrazines and pyridines	22	0.09	0.89	0.98	0.91	0.81	1.05	0.35
Nitriles	5	0.06	0.47	0.5	1	0.96	3.3	8.78
Nitro compounds	6	2.18	2.18	2.18	0.95	0.96	0.97	2.08
Nitrooxy compounds	8	0.42	0.54	0.59	0.98	0.99	1.19	1.07
Amides	5	1.38	1.38	1.43	0.81	0.88	0.72	-1.23
Thioethers	8	0.35	0.43	0.51	0.99	0.97	1.73	1.56
Thiols	4	-0.5	0.5	0.53	1	0.97	3.2	1.93

Aliphatic chain + fluorine	3	-1.58	1.58	1.77	0.97	0.91	0.56	-1.17
Aromatic ring + fluorine	2	-1.93	1.93	2.05	-1	-1	-1.47	-3.23
Phosphoryl	2	-1.27	1.27	1.36	1	1	1.81	5.26
Sulfone	2	-1.23	1.23	1.74	1	1	0.3	-6
Sum	394	-0.27	0.95	1.2	0.91	0.91	0.91	-0.48

Table S4 The performance of MM-PBSA (PB_DELPHI) using RESP charge model before atom radii optimization.

Training set molecules excludes molecules with multiple functional groups. The unit of MSE, MUE and RMSE is kcal/mol.

Subclass	**Number**	**MSE**	**MUE**	**RMSE**	**PI**	**R**	**k**	**b**
Non-cyclic alkanes	25	-0.43	0.44	0.53	0.62	0.65	0.72	0.28
Cycloalkanes	9	0.45	0.5	0.61	0.55	0.72	0.82	0.75
Alkenes	22	-0.9	1.12	1.24	0.15	0.26	0.41	-0.19
Alkynes	6	-1.95	1.95	1.96	0.96	0.94	0.64	-1.89
Aromatic hydrocarbons	36	-0.41	0.57	0.68	0.85	0.89	0.87	-0.62
Aliphatic chain + chloride	22	-0.79	1.2	1.38	0.75	0.71	1.36	-0.53
Aromatic ring + chloride	24	0.91	1.65	2.15	0.03	0.01	0.01	-1.13
Aliphatic chain + bromide	14	-0.1	0.38	0.49	0.86	0.87	0.66	-0.28
Aromatic ring + bromide	4	0.09	0.79	1.07	0.08	0.44	1.13	0.34
Hydrocarbon + iodide	10	-0.14	0.48	0.57	0.83	0.8	0.38	-0.57
Ethers	14	-0.4	0.9	1.31	0.71	0.72	1.08	-0.21
Alkyl alcohols	25	-1.62	1.62	1.96	0.89	0.98	1.48	0.74
Alkene + alcohols	3	-1.48	1.48	1.51	1	0.99	2.22	4.33
Phenols	17	-0.64	0.75	0.91	0.59	0.71	0.91	-1.22
Ketones	19	-1.79	1.79	1.86	0.71	0.81	1.01	-1.75
Aldehydes	10	-2.08	2.08	2.09	0.83	0.84	0.79	-2.69
Esters	34	-4.4	4.4	4.71	0.86	0.97	2.01	-1.35
Amines	25	2.06	2.15	2.83	0.4	0.49	0.67	0.49
Anilines	8	0.48	0.5	0.53	0.99	0.98	1.02	0.56

Pyrazines and pyridines	22	0.88	1.24	1.33	0.64	0.81	1.08	1.31
Nitriles	5	-0.92	0.92	1.01	1	0.94	2.82	6
Nitro compounds	6	-4.09	4.09	4.1	1	0.99	1.67	-1.83
Nitrooxy compounds	8	-4.9	4.9	5.27	0.95	0.97	2.13	-1.07
Amides	5	-0.4	0.61	0.79	0.67	0.72	0.94	-0.92
Thioethers	8	0.13	0.74	0.83	0.48	0.33	0.64	-0.47
Thiols	4	-0.75	0.75	0.85	0.13	-0.05	-0.24	-2.12
Aliphatic chain + fluorine	3	-2.15	2.15	2.2	0.97	0.96	0.83	-2
Aromatic ring + fluorine	2	-1.93	1.93	1.96	-1	-1	-0.28	-2.6
Phosphoryl	2	-3.64	3.64	3.68	1	1	1.89	3.6
Sulfone	2	-5.83	5.83	5.84	1	1	1.19	-4.55
Sum	394	-0.87	1.58	2.23	0.83	0.82	1.05	-0.74

Table S5 The performance of MM-PBSA (PB_DELPHI) using RESP charge model after atom radii optimization.

Training set molecules excludes molecules with multiple functional groups. The unit of MSE, MUE and RMSE is kcal/mol.

Subclass	**Number**	**MSE**	**MUE**	**RMSE**	**PI**	**R**	**k**	**b**
Non-cyclic alkanes	25	-0.94	0.94	0.99	0.7	0.72	0.97	-0.86
Cycloalkanes	9	-0.05	0.33	0.44	0.58	0.76	0.98	-0.02
Alkenes	22	-1.49	1.56	1.73	0.2	0.29	0.49	-0.87
Alkynes	6	-2.09	2.09	2.1	0.96	0.98	0.86	-2.07
Aromatic hydrocarbons	36	-0.98	0.98	1.13	0.87	0.89	0.89	-1.15
Aliphatic chain + chloride	22	-0.81	0.89	1.04	0.86	0.83	1.19	-0.67
Aromatic ring + chloride	24	0.07	1.24	1.47	0.22	0.13	0.17	-1.65
Aliphatic chain + bromide	14	-0.99	0.99	1.06	0.9	0.92	0.92	-1.03
Aromatic ring + bromide	4	-0.99	1.05	1.3	0.08	0.57	1.26	-0.5
Hydrocarbon + iodide	10	-1.25	1.25	1.28	0.98	0.96	0.76	-1.42

Ethers	14	0.11	0.9	1.04	0.73	0.72	0.9	-0.12
Alkyl alcohols	25	0.01	0.33	0.49	0.94	0.99	1.17	0.85
Alkene + alcohols	3	-0.13	0.35	0.45	1	0.96	2.61	7.53
Phenols	17	-0.06	0.45	0.56	0.65	0.77	0.93	-0.52
Ketones	19	-0.51	0.64	0.73	0.77	0.85	1.18	0.07
Aldehydes	10	-0.97	0.97	1.01	0.76	0.84	1	-0.96
Esters	34	-2.2	2.2	2.38	0.88	0.96	1.43	-0.89
Amines	25	1.54	1.87	2.5	0.39	0.49	0.68	0.01
Anilines	8	-0.14	0.18	0.29	0.99	0.98	1.03	0.03
Pyrazines and pyridines	22	0.21	0.86	1.04	0.66	0.81	1.1	0.71
Nitriles	5	-1.63	1.63	1.71	1	0.94	3.18	6.64
Nitro compounds	6	-1.24	1.24	1.28	1	0.99	1.73	1.21
Nitrooxy compounds	8	-1.81	1.81	2.03	0.95	0.98	1.52	-0.05
Amides	5	1.33	1.33	1.48	0.81	0.74	0.95	0.86
Thioethers	8	0.03	0.53	0.61	0.48	0.6	1.02	0.07
Thiols	4	-0.86	0.86	0.92	0.58	0.27	1.12	-0.73
Aliphatic chain + fluorine	3	-1.76	1.76	1.84	0.97	0.97	0.71	-1.49
Aromatic ring + fluorine	2	-1.88	1.88	1.89	1	1	0.16	-2.32
Phosphoryl	2	-0.23	0.36	0.43	1	1	1.6	4.64
Sulfone	2	-2.02	2.02	2.19	1	1	0.52	-5.3
Sum	394	-0.62	1.12	1.43	0.88	0.89	0.86	-0.95

Table S6 The old and updated PB radii parameters for different atom types and the parameters for WSAS calculation.

Atom type	Radii before optimization	Radii after optimization	Parameters for WSAS	Weight applied to WSAS
Hydrogen				
h1	1.19	1.19	1.20	0.105257
h2	1.19	1.19	1.20	0.0866113
h3	1.19	1.19	1.20	0.0708034
h4	1.19	1.19	1.20	0.104611
h5	1.19	1.19	1.20	0.0951559
ha	1.19	1.19	1.20	0.114837
hc	1.19	1.19	1.20	0.127134
hn	1.19	1.19	1.20	0.0145069
hn1		1.50	1.20	0.0145069
hn2		1.60	1.20	0.0145069

hn3		1.70	1.20	0.0145069
ho	1.19	1.19	1.20	0.004208
hp	1.19	1.19	1.20	0.0166403
hs	1.19	1.19	1.20	0.0157608
hw	1.19	1.19	1.20	0.0106
hx	1.19	1.19	1.20	0.0574766
HC	1.19	1.19	1.20	0.127134
HA	1.19	1.19	1.20	0.114837
HO	1.19	1.19	1.20	0.004208
HS	1.19	1.19	1.20	0.0157608
HW	1.19	1.19	1.20	0.004208
HP	1.19	1.19	1.20	0.0166403
HZ	1.19	1.19		
H1	1.19	1.19	1.20	0.105257
H2	1.19	1.19	1.20	0.0866113
H3	1.19	1.19	1.20	0.0708034
H4	1.19	1.19	1.20	0.104611
H5	1.19	1.19	1.20	0.0951559
H	1.19	1.19	1.20	0.0145069
Carbon				
c	1.76	1.76	1.70	0.559732
c1	1.76	1.90	1.70	0.826582
c2	1.76	1.76	1.70	0.559732
c3	1.76	1.76	1.70	0.63088
ca	1.76	1.76	1.70	0.559732
cp	1.76	1.76	1.70	0.559732
cq	1.76	1.76	1.70	0.559732
cc	1.76	1.76	1.70	0.559732
cd	1.76	1.76	1.70	0.559732
ce	1.76	1.76	1.70	0.559732
cf	1.76	1.76	1.70	0.559732
cg	1.76	1.76	1.70	0.826582
ch	1.76	1.76	1.70	0.826582
cx	1.76	1.76	1.70	0.63088
cy	1.76	1.76	1.70	0.63088
cz	1.76	1.76	1.70	0.559732
c5	1.76	1.76	1.70	0.63088
c6	1.76	1.76	1.70	0.63088
cu	1.76	1.76	1.70	0.559732
cv	1.76	1.76	1.70	0.559732
CA	1.76	1.76	1.70	0.559732
CB	1.76	1.76	1.70	0.559732
CC	1.76	1.76	1.70	0.559732
CD	1.76	1.76	1.70	0.559732
CK	1.76	1.76	1.70	0.559732

CM	1.76	1.76	1.70	0.559732
CN	1.76	1.76	1.70	0.559732
CQ	1.76	1.76	1.70	0.559732
CR	1.76	1.76	1.70	0.559732
CT	1.76	1.76	1.70	0.63088
CV	1.76	1.76	1.70	0.559732
CW	1.76	1.76	1.70	0.559732
C*	1.76	1.76	1.70	0.559732
CY	1.76	1.76	1.70	0.826582
CZ	1.76	1.76	1.70	0.826582
C	1.76	1.76	1.70	0.826582
C3	1.76	1.76	1.70	0.63088
C4	1.76	1.76	1.70	0.63088
C5	1.76	1.76	1.70	0.559732
C6	1.76	1.76	1.70	0.559732
C8	1.76	1.76	1.70	0.63088
CX	1.76	1.76	1.70	0.63088
2C	1.76	1.76	1.70	0.63088
3C	1.76	1.76	1.70	0.63088
CO	1.76	1.76	1.70	0.559732
CI	1.76	1.76	1.70	0.63088
CP	1.76	1.76	1.70	0.559732
CS	1.76	1.76	1.70	0.559732
Nitrogen				
n	1.73	1.73	1.55	0.635011
n1	1.73	1.73	1.55	0.567605
n2	1.73	1.73	1.55	0.582155
n3	1.73	1.73	1.55	0.546228
n4	1.73	1.73	1.55	1.56076
n5	1.73	1.73	1.55	0.485127
n6	1.73	1.73	1.55	0.485127
n7	1.73	1.73	1.55	0.485127
n8	1.73	1.73	1.55	0.433329
n9	1.73	1.73	1.55	0.329614
na	1.73	1.73	1.55	0.72638
nb	1.73	1.73	1.55	0.582155
nc	1.73	1.73	1.55	0.582155
nd	1.73	1.73	1.55	0.582155
ne	1.73	1.73	1.55	0.582155
nf	1.73	1.73	1.55	0.582155
nh	1.73	1.73	1.55	0.734254
no	1.73	1.73	1.55	0.546228
ni	1.73	1.73	1.55	0.635011
nj	1.73	1.73	1.55	0.635011
nk	1.73	1.73	1.55	1.38946

nl	1.73	1.73	1.55	1.38946
nm	1.73	1.73	1.55	0.734254
nn	1.73	1.73	1.55	0.734254
np	1.73	1.73	1.55	0.546228
nq	1.73	1.73	1.55	0.546228
ns	1.73	1.73	1.55	0.584969
nt	1.73	1.73	1.55	0.540968
nu	1.73	1.73	1.55	0.676782
nv	1.73	1.73	1.55	0.625821
nx	1.73	1.73	1.55	1.38946
ny	1.73	1.73	1.55	1.24398
nz	1.73	1.73	1.55	1.11956
n+	1.73	1.73	1.55	1.01253
NA	1.73	1.73	1.55	0.72638
NB	1.73	1.73	1.55	0.582155
NC	1.73	1.73	1.55	0.582155
N2	1.73	1.73	1.55	0.72638
N3	1.73	1.73	1.55	0.546228
NT	1.73	1.73	1.55	0.546228
N*	1.73	1.73	1.55	0.72638
NY	1.73	1.73	1.55	0.567605
N	1.73	1.73	1.55	0.635011
Oxygen				
o	1.43	1.70	1.52	0.528811
on		2.00	1.52	0.528811
oi		1.28	1.52	0.528811
oh	1.43	1.70	1.52	0.507605
os	1.43	1.64	1.52	0.413186
ow	1.43	1.64	1.52	0.594825
op	1.43	1.64	1.52	0.413186
oq	1.43	1.64	1.52	0.413186
O2	1.43	1.64	1.52	0.528811
OH	1.43	1.64	1.52	0.507605
OS	1.43	1.64	1.52	0.413186
OW	1.43	1.64	1.52	0.507605
O	1.43	1.64	1.52	0.528811
Sulfur				
s	1.75	2.00	1.80	1.15379
s2	1.75	2.00	1.80	1.15379
s4	1.75	2.00	1.80	1.15379
s6	1.75	2.80	1.80	0.847601
sh	1.75	2.00	1.80	1.15379
ss	1.75	2.00	1.80	1.15379
sx	1.75	2.00	1.80	1.15379
sy	1.75	2.00	1.80	0.847601

sp	1.75	2.00	1.80	1.15379
sq	1.75	2.00	1.80	1.15379
SH	1.75	2.00	1.80	1.15379
S	1.75	2.00	1.80	1.15379
Phosphate				
p2	1.75	2.00	1.80	1.20046
p3	1.75	2.00	1.80	1.20046
p4	1.75	2.00	1.80	1.20046
p5	1.75	2.60	1.80	1.20046
pb	1.75	2.00	1.80	1.20046
pc	1.75	2.00	1.80	1.20046
pd	1.75	2.00	1.80	1.20046
pe	1.75	2.00	1.80	1.20046
pf	1.75	2.00	1.80	1.20046
px	1.75	2.00	1.80	1.20046
py	1.75	2.00	1.80	1.20046
p	1.75	2.00		
P	1.75	2.00	1.80	1.20046
Halid				
f	1.40	1.90	1.47	0.393452
F	1.40	1.90	1.47	0.393452
cl	1.54	2.10	1.75	1.05024
Cl	1.54	2.10	1.75	1.05024
CL	1.54	2.10		
br	1.99	2.15	1.85	1.46244
Br	1.99	2.15	1.85	1.46244
BR	1.99	2.15		
i	2.00	2.20	1.90	2.00408
I	2.00	2.20	1.90	2.00408
Boron				
B	1.50	1.50		
Metal				
Mn	2.00	2.00		
Mg	2.00	2.00		
Fe	2.00	2.00		
Lone pair				
lp	0.00	0.00		
LP	0.00	0.00		
Z5	1.76	1.76	1.70	

Bibliography

1. Skyner, R.E., et al., *A review of methods for the calculation of solution free energies and the modelling of systems in solution.* Phys Chem Chem Phys, 2015. **17**(9): p. 6174-91.
2. Procacci, P., *Solvation free energies via alchemical simulations: let's get honest about sampling, once more.* Phys Chem Chem Phys, 2019. **21**(25): p. 13826-13834.
3. Genheden, S. and U. Ryde, *The MM/PBSA and MM/GBSA methods to estimate ligand-binding affinities.* Expert Opin Drug Discov, 2015. **10**(5): p. 449-61.
4. Wang, E., et al., *End-Point Binding Free Energy Calculation with MM/PBSA and MM/GBSA: Strategies and Applications in Drug Design.* Chem Rev, 2019. **119**(16): p. 9478-9508.
5. Cramer, C.J. and D.G. Truhlar, *An SCF Solvation Model for the Hydrophobic Effect and Absolute Free Energies of Aqueous Solvation.* Science, 1992. **256**(5054): p. 213-217.
6. Wang, J., T. Hou, and X. Xu, *Recent Advances in Free Energy Calculations with a Combination of Molecular Mechanics and Continuum Models.* Current Computer - Aided Drug Design, 2006. **2**(3): p. 287-306.
7. Izairi, R. and H. Kamberaj, *Comparison Study of Polar and Nonpolar Contributions to Solvation Free Energy.* J Chem Inf Model, 2017. **57**(10): p. 2539-2553.
8. Tuccinardi, T., *What is the current value of MM/PBSA and MM/GBSA methods in drug discovery?* Expert Opin Drug Discov, 2021: p. 1-5.
9. Lafont, V., et al., *Protein-protein recognition and interaction hot spots in an antigen-antibody complex: free energy decomposition identifies "efficient amino acids".* Proteins, 2007. **67**(2): p. 418-34.
10. Poli, G., et al., *Application of MM-PBSA Methods in Virtual Screening.* Molecules, 2020. **25**(8).
11. Lazaridis, T., *Binding Affinity and Specificity from Computational Studies.* Current Organic Chemistry, 2002. **6**(14): p. 14.
12. Hou, T., et al., *Assessing the Performance of the MM/PBSA and MM/GBSA Methods. 1. The Accuracy of Binding Free Energy Calculations Based on Molecular Dynamics Simulations.* Journal of Chemical Information and Modeling, 2011. **51**(1): p. 69-82.
13. Xu, L., et al., *Assessing the Performance of MM/PBSA and MM/GBSA Methods. 3. The Impact of Force Fields and Ligand Charge Models.* The Journal of Physical Chemistry B, 2013. **117**(28): p. 8408-8421.
14. D.A. Case, I.Y.B.-S., S.R. Brozell, D.S. Cerutti, T.E. Cheatham, III, V.W.D. Cruzeiro, T.A. Darden, R.E. Duke, D. Ghoreishi, M.K. Gilson, H. Gohlke, A.W. Goetz, D. Greene, R Harris, N. Homeyer, Y. Huang, S. Izadi, A. Kovalenko, T. Kurtzman, T.S. Lee, S. LeGrand, P. Li, C. Lin, J. Liu, T. Luchko, R. Luo, D.J. Mermelstein, K.M. Merz, Y. Miao, G. Monard, C. Nguyen, H. Nguyen, I. Omelyan, A. Onufriev, F. Pan, R. Qi, D.R. Roe, A. Roitberg, C. Sagui, S. Schott-Verdugo, J. Shen, C.L. Simmerling, J. Smith, R. SalomonFerrer, J. Swails, R.C. Walker, J. Wang, H. Wei, R.M. Wolf, X. Wu, L. Xiao, D.M. York and P.A. Kollman, *AMBER 2018*. 2018, University of California, San Francisco: San Francisco.
15. Tan, C., Y.H. Tan, and R. Luo, *Implicit nonpolar solvent models.* J Phys Chem B, 2007. **111**(42): p. 12263-74.

16. Fu, T., et al., *Binding free energy estimation for protein-ligand complex based on MM-PBSA with various partial charge models.* Curr Pharm Des, 2013. **19**(12): p. 2293-307.
17. Bayly, C.I., et al., *A well-behaved electrostatic potential based method using charge restraints for deriving atomic charges: the RESP model.* The Journal of Physical Chemistry, 1993. **97**(40): p. 10269-10280.
18. Wang, J., P. Cieplak, and P.A. Kollman, *How well does a restrained electrostatic potential (RESP) model perform in calculating conformational energies of organic and biological molecules?* Journal of Computational Chemistry, 2000. **21**(12): p. 1049-1074.
19. Wang, J., et al., *Development and testing of a general amber force field.* J Comput Chem, 2004. **25**(9): p. 1157-1174.
20. Jakalian, A., D.B. Jack, and C.I. Bayly, *Fast, efficient generation of high-quality atomic charges. AM1-BCC model: II. Parameterization and validation.* J Comput Chem, 2002. **23**(16): p. 1623-41.
21. Araz Jakalian, B.L.B., David B. Jack, Christopher I. Bayly, *Fast, efficient generation of high-quality atomic charges. AM1-BCC model: I. Method.* J Comput Chem, 2000. **21**(2): p. 15.
22. He, X., et al., *A fast and high-quality charge model for the next generation general AMBER force field.* J Chem Phys, 2020. **153**(11): p. 114502.
23. Bruckner, S. and S. Boresch, *Efficiency of alchemical free energy simulations. I. A practical comparison of the exponential formula, thermodynamic integration, and Bennett's acceptance ratio method.* Journal of Computational Chemistry, 2011. **32**(7): p. 1303-1319.
24. Hughes, J.D., et al., *Physiochemical drug properties associated with in vivo toxicological outcomes.* Bioorganic & Medicinal Chemistry Letters, 2008. **18**(17): p. 4872-4875.
25. Waring, M.J., *Defining optimum lipophilicity and molecular weight ranges for drug candidates—Molecular weight dependent lower logD limits based on permeability.* Bioorganic & Medicinal Chemistry Letters, 2009. **19**(10): p. 2844-2851.
26. Gleeson, M.P., *Generation of a Set of Simple, Interpretable ADMET Rules of Thumb*. Journal of Medicinal Chemistry, 2008. **51**(4): p. 817-834.
27. Johnson, T.W., K.R. Dress, and M. Edwards, *Using the Golden Triangle to optimize clearance and oral absorption.* Bioorganic & Medicinal Chemistry Letters, 2009. **19**(19): p. 5560-5564.
28. Fujita, T., J. Iwasa, and C. Hansch, *A New Substituent Constant, π, Derived from Partition Coefficients.* Journal of the American Chemical Society, 1964. **86**(23): p. 5175-5180.
29. Iwasa, J., T. Fujita, and C. Hansch, *Substituent constants for aliphatic functions obtained from partition coefficients.* Journal of Medicinal Chemistry, 1965. **8**(2): p. 150-153.
30. Lipinski, C.A., et al., *Experimental and computational approaches to estimate solubility and permeability in drug discovery and development settings.* Adv Drug Deliv Rev, 2001. **46**(1-3): p. 3-26.
31. Lipinski, C.A., *Lead- and drug-like compounds: the rule-of-five revolution.* Drug Discov Today Technol, 2004. **1**(4): p. 337-41.
32. Sangster, J., *Octanol-Water Partition Coefficients of Simple Organic Compounds.* Journal of Physical and Chemical Reference Data, 1989. **18**(3): p. 1111-1229.
33. Leo, A., C. Hansch, and D. Elkins, *Partition coefficients and their uses.* Chemical Reviews, 1971. **71**(6): p. 525-616.

34. Arup Ghose, V.V., *Combinatorial Library Design and Evaluation: Principles, Software, Tools, and Applications in Drug Discovery*. 2001: CRC Press.
35. Waterbeemd, H.v.d., *Chemometric Methods in Molecular Design*. 2008: John Wiley & Sons.
36. Liao, Q., J. Yao, and S. Yuan, *SVM approach for predicting LogP.* Molecular Diversity, 2006. **10**(3): p. 301-309.
37. Ghose, A.K., A. Pritchett, and G.M. Crippen, *Atomic physicochemical parameters for three dimensional structure directed quantitative structure-activity relationships III: Modeling hydrophobic interactions.* Journal of Computational Chemistry, 1988. **9**(1): p. 80-90.
38. Wang, Y., J.W. Godden, and J. Bajorath, *A novel Descriptor histogram filtering method for database mining and the identification of active molecules.* Letters in Drug Design & Discovery, 2007. **4**(4): p. 286-292.
39. Wildman, S.A. and G.M. Crippen, *Prediction of Physicochemical Parameters by Atomic Contributions.* Journal of Chemical Information and Computer Sciences, 1999. **39**(5): p. 868-873.
40. Tetko, I.V. and V.Y. Tanchuk, *Application of Associative Neural Networks for Prediction of Lipophilicity in ALOGPS 2.1 Program.* Journal of Chemical Information and Computer Sciences, 2002. **42**(5): p. 1136-1145.
41. Leo, A.J. and D. Hoekman, *Calculating log P(oct) with no missing fragments;The problem of estimating new interaction parameters.* Perspectives in Drug Discovery and Design, 2000. **18**(1): p. 19-38.
42. Klopman, G., et al., *Computer automated log P calculations based on an extended group contribution approach.* Journal of Chemical Information and Computer Sciences, 1994. **34**(4): p. 752-781.
43. Tetko, I.V. and G.I. Poda, *Prediction of Log P with Property-Based Methods*, in *Molecular Drug Properties*. 2007. p. 381-406.
44. Procacci, P. and G. Guarnieri, *SAMPL6 blind predictions of water-octanol partition coefficients using nonequilibrium alchemical approaches.* Journal of Computer-Aided Molecular Design, 2020. **34**(4): p. 371-384.
45. Bryant, M.J., et al., *The CSD Drug Subset: The Changing Chemistry and Crystallography of Small Molecule Pharmaceuticals.* Journal of Pharmaceutical Sciences, 2019. **108**(5): p. 1655-1662.
46. Shultz, M.D., *Two Decades under the Influence of the Rule of Five and the Changing Properties of Approved Oral Drugs.* Journal of Medicinal Chemistry, 2019. **62**(4): p. 1701-1714.
47. Pozzan, A., *QM Calculations in ADMET Prediction*, in *Quantum Mechanics in Drug Discovery*, A. Heifetz, Editor. 2020, Springer US: New York, NY. p. 285-305.
48. Işık, M., et al., *Assessing the accuracy of octanol–water partition coefficient predictions in the SAMPL6 Part II log P Challenge*. Journal of Computer-Aided Molecular Design, 2020. **34**(4): p. 335-370.
49. Wang, L., et al., *Accurate and reliable prediction of relative ligand binding potency in prospective drug discovery by way of a modern free-energy calculation protocol and force field.* J Am Chem Soc, 2015. **137**(7): p. 2695-2703.
50. He, X., et al., *Fast, Accurate, and Reliable Protocols for Routine Calculations of Protein-Ligand Binding Affinities in Drug Design Projects Using AMBER GPU-TI with ff14SB/GAFF*. ACS Omega, 2020. **5**(9): p. 4611-4619.

51. Hao, D., et al., *How Well Does the Extended Linear Interaction Energy Method Perform in Accurate Binding Free Energy Calculations?* J Chem Inf Model, 2020. **60**(12): p. 6624-6633.
52. Cumming, J.N., et al., *Structure based design of iminohydantoin BACE1 inhibitors: Identification of an orally available, centrally active BACE1 inhibitor.* Bioorganic & Medicinal Chemistry Letters, 2012. **22**(7): p. 2444-2449.
53. Szczepankiewicz, B.G., et al., *Aminopyridine-Based c-Jun N-Terminal Kinase Inhibitors with Cellular Activity and Minimal Cross-Kinase Activity.* Journal of Medicinal Chemistry, 2006. **49**(12): p. 3563-3580.
54. Goldstein, D.M., et al., *Discovery of 6-(2,4-Difluorophenoxy)-2-[3-hydroxy-1-(2-hydroxyethyl)propylamino]-8-methyl-8H-pyrido[2,3-d]pyrimidin-7-one (Pamapimod) and 6-(2,4-Difluorophenoxy)-8-methyl-2-(tetrahydro-2H-pyran-4-ylamino)pyrido[2,3-d]pyrimidin-7(8H)-one (R1487) as Orally Bioavailable and Highly Selective Inhibitors of p38α Mitogen-Activated Protein Kinase.* Journal of Medicinal Chemistry, 2011. **54**(7): p. 2255-2265.
55. Wilson, D.P., et al., *Structure-Based Optimization of Protein Tyrosine Phosphatase 1B Inhibitors: From the Active Site to the Second Phosphotyrosine Binding Site.* Journal of Medicinal Chemistry, 2007. **50**(19): p. 4681-4698.
56. Bannan, C.C., et al., *Calculating Partition Coefficients of Small Molecules in Octanol/Water and Cyclohexane/Water.* Journal of Chemical Theory and Computation, 2016. **12**(8): p. 4015-4024.
57. Rocchia, W., E. Alexov, and B. Honig, *Extending the Applicability of the Nonlinear Poisson−Boltzmann Equation: Multiple Dielectric Constants and Multivalent Ions.* The Journal of Physical Chemistry B, 2001. **105**(28): p. 6507-6514.
58. Li, L., et al., *DelPhi: a comprehensive suite for DelPhi software and associated resources.* BMC Biophys, 2012. **5**: p. 9.
59. Mobley, D.L. and J.P. Guthrie, *FreeSolv: a database of experimental and calculated hydration free energies, with input files.* Journal of Computer-Aided Molecular Design, 2014. **28**(7): p. 711-720.
60. Marenich, A.V.K., C. P.; Thompson, J. D.; Hawkins, G. D.; Chambers, C. C.; Giesen, D. J.; Winget, P.; Cramer, C. J.; Truhlar, D. G., *Minnesota Solvation Database – version 2012*. 2012.
61. Frisch, M.J.T., G. W.; Schlegel, H. B.; Scuseria, G. E.; Robb, M. A.; Cheeseman, J. R.; Scalmani, G.; Barone, V.; Petersson, G. A.; Nakatsuji, H.; Li, X.; Caricato, M.; Marenich, A. V.; Bloino, J.; Janesko, B. G.; Gomperts, R.; Mennucci, B.; Hratchian, H. P.; Ortiz, J. V.; Izmaylov, A. F.; Sonnenberg, J. L.; Williams-Young, D.; Ding, F.; Lipparini, F.; Egidi, F.; Goings, J.; Peng, B.; Petrone, A.; Henderson, T.; Ranasinghe, D.; Zakrzewski, V. G.; Gao, J.; Rega, N.; Zheng, G.; Liang, W.; Hada, M.; Ehara, M.; Toyota, K.; Fukuda, R.; Hasegawa, J.; Ishida, M.; Nakajima, T.; Honda, Y.; Kitao, O.; Nakai, H.; Vreven, T.; Throssell, K.; Montgomery, J. A., Jr.; Peralta, J. E.; Ogliaro, F.; Bearpark, M. J.; Heyd, J. J.; Brothers, E. N.; Kudin, K. N.; Staroverov, V. N.; Keith, T. A.; Kobayashi, R.; Normand, J.; Raghavachari, K.; Rendell, A. P.; Burant, J. C.; Iyengar, S. S.; Tomasi, J.; Cossi, M.; Millam, J. M.; Klene, M.; Adamo, C.; Cammi, R.; Ochterski, J. W.; Martin, R. L.; Morokuma, K.; Farkas, O.; Foresman, J. B.; Fox, D. J. , *Gaussian 16 Rev. C.01*. 2016, Gaussian, Inc.: Wallingford, CT.

62. Jorgensen, W.L., et al., *Comparison of simple potential functions for simulating liquid water.* The Journal of Chemical Physics, 1983. **79**(2): p. 926-935.
63. Larini, L., R. Mannella, and D. Leporini, *Langevin stabilization of molecular-dynamics simulations of polymers by means of quasisymplectic algorithms.* J Chem Phys, 2007. **126**(10): p. 104101.
64. Roe, D.R. and T.E. Cheatham, *PTRAJ and CPPTRAJ: Software for Processing and Analysis of Molecular Dynamics Trajectory Data.* Journal of Chemical Theory and Computation, 2013. **9**(7): p. 3084-3095.
65. Lee, T.S., et al., *GPU-Accelerated Molecular Dynamics and Free Energy Methods in Amber18: Performance Enhancements and New Features.* J Chem Inf Model, 2018. **58**(10): p. 2043-2050.
66. Lee, T.S., et al., *Toward Fast and Accurate Binding Affinity Prediction with pmemdGTI: An Efficient Implementation of GPU-Accelerated Thermodynamic Integration.* J Chem Theory Comput, 2017. **13**(7): p. 3077-3084.
67. Homeyer, N., et al., *Binding Free Energy Calculations for Lead Optimization: Assessment of Their Accuracy in an Industrial Drug Design Context.* Journal of Chemical Theory and Computation, 2014. **10**(8): p. 3331-3344.
68. Steinbrecher, T., I. Joung, and D.A. Case, *Soft-core potentials in thermodynamic integration: comparing one- and two-step transformations.* J Comput Chem, 2011. **32**(15): p. 3253-63.
69. Pearlman, D.A. and P.S. Charifson, *Are free energy calculations useful in practice? A comparison with rapid scoring functions for the p38 MAP kinase protein system.* J Med Chem, 2001. **44**(21): p. 3417-23.
70. Song, L.F., et al., *Using AMBER18 for Relative Free Energy Calculations.* J Chem Inf Model, 2019. **59**(7): p. 3128-3135.
71. Michel, J., M.L. Verdonk, and J.W. Essex, *Protein-ligand binding affinity predictions by implicit solvent simulations: a tool for lead optimization?* J Med Chem, 2006. **49**(25): p. 7427-39.
72. Wang, J.M., T.J. Hou, and X.J. Xu, *Recent Advances in Free Energy Calculations with a Combination of Molecular Mechanics and Continuum Models.* Curr Comput Aided Drug Des, 2006. **2**(3): p. 287-306.
73. Wang, J. and T. Hou, *Develop and test a solvent accessible surface area-based model in conformational entropy calculations.* J Chem Inf Model, 2012. **52**(5): p. 1199-212.
74. Sterling, T. and J.J. Irwin, *ZINC 15 – Ligand Discovery for Everyone.* Journal of Chemical Information and Modeling, 2015. **55**(11): p. 2324-2337.
75. O'Boyle, N.M., et al., *Open Babel: An open chemical toolbox.* Journal of Cheminformatics, 2011. **3**(1): p. 33.
76. Borhani, T.N., et al., *Hybrid QSPR models for the prediction of the free energy of solvation of organic solute/solvent pairs.* Phys Chem Chem Phys, 2019. **21**(25): p. 13706-13720.
77. Harder, E., et al., *OPLS3: A Force Field Providing Broad Coverage of Drug-like Small Molecules and Proteins.* J Chem Theory Comput, 2016. **12**(1): p. 281-96.
78. Nicholls, A., et al., *Predicting Small-Molecule Solvation Free Energies: An Informal Blind Test for Computational Chemistry.* Journal of Medicinal Chemistry, 2008. **51**(4): p. 769-779.
79. Frisch, M.J.T., G. W.; Schlegel, H. B.; Scuseria, G. E.; Robb, M. A.; Cheeseman, J. R.; Montgomery, Jr., J. A.; Vreven, T.; Kudin, K. N.; Burant, J. C.; Millam, J. M.; Iyengar, S.

S.; Tomasi, J.; Barone, V.; Mennucci, B.; Cossi, M.; Scalmani, G.; Rega, N.; Petersson, G. A.; Nakatsuji, H.; Hada, M.; Ehara, M.; Toyota, K.; Fukuda, R.; Hasegawa, J.; Ishida, M.; Nakajima, T.; Honda, Y.; Kitao, O.; Nakai, H.; Klene, M.; Li, X.; Knox, J. E.; Hratchian, H. P.; Cross, J. B.; Bakken, V.; Adamo, C.; Jaramillo, J.; Gomperts, R.; Stratmann, R. E.; Yazyev, O.; Austin, J.; Cammi, R.; Pomelli, C.; Ochterski, J. W.; Ayala, P. Y.; Morokuma, K.; Voth, G. A.; Salvador, P.; Dannenberg, J. J.; Zakrzewski, V. G.; Dapprich, S.; Daniels, A. D.; Strain, M. C.; Farkas, O.; Malick, D. K.; Rabuck, D.; Raghavachari, K.; Foresman, J. B.; Ortiz, J. V.; Cui, Q.; Baboul, A. G.; Clifford, S.; Cioslowski, J.; Stefanov, B. B.; Liu, G.; Liashenko, A.; Piskorz, P.; Komaromi, I.; Martin, R. L.; Fox, D. J.; Keith, T.; Al-Laham, M. A.; Peng, C. Y.; Nanayakkara, A.; Challacombe, M.; Gill, P. M. W.; Johnson, B.; Chen, W.; Wong, M. W.; Gonzalez, C.; Pople, J. A. , *Gaussian 03*. 2004, Gaussian Inc.:: Wallingford, CT.

80. Grant, J.A., B.T. Pickup, and A. Nicholls, *A smooth permittivity function for Poisson–Boltzmann solvation methods.* Journal of Computational Chemistry, 2001. **22**(6): p. 608-640.
81. Sitkoff, D., K.A. Sharp, and B. Honig, *Accurate Calculation of Hydration Free Energies Using Macroscopic Solvent Models.* The Journal of Physical Chemistry, 1994. **98**(7): p. 1978-1988.
82. Marenich, A.V.K., C. P.; Thompson, J. D.; Hawkins, G. D.; Chambers, C. C.; Giesen, D. J.; and P.C. Winget, C. J.; Truhlar, D. G., *Minnesota Solvation Database – version 2012*, M. University of Minnesota, Editor. 2012.
83. Lennard-Jones, J.E., *Cohesion.* Proceedings of the Physical Society, 1931. **43**(5): p. 461-482.
84. Jones, J.E. and S. Chapman, *On the determination of molecular fields.—I. From the variation of the viscosity of a gas with temperature.* Proceedings of the Royal Society of London. Series A, Containing Papers of a Mathematical and Physical Character, 1924. **106**(738): p. 441-462.
85. Jones, J.E. and S. Chapman, *On the determination of molecular fields. —II. From the equation of state of a gas.* Proceedings of the Royal Society of London. Series A, Containing Papers of a Mathematical and Physical Character, 1924. **106**(738): p. 463-477.